

1 The optimal tuning, within carbon limits, of thermal mass in naturally  
2 ventilated buildings

3 Salmaan Craig<sup>a,\*</sup>

4 <sup>a</sup>*School of Architecture, McGill University, Montréal, QC, Canada*

---

5 **Abstract**

This paper shows how to optimize the physical proportions of a building so that it synchronizes ambient heat exchanges in a natural feedback cycle. The internal mass is thermally coupled with buoyancy ventilation; the cycle is driven by the daily swing of outdoor temperature. Integrating functions in this way—so that structural materials can reliably cool and power the ventilation for buildings—could help decarbonize the construction industry and provide an effective strategy for adapting to life-threatening heatwaves. Based on harmonic analysis, the method allows designers to thermally tune the form and mass of a building to meet chosen targets for temperature and ventilation in free-running mode. Once the optimal balance of exchange rates is known, design teams can proportionally adjust the building height and ventilation openings versus the surface area and thickness of an internal thermal mass. The possible permutations are infinite but parametrically constrained, allowing teams to fairly compare the functional and environmental credentials of different construction materials while they produce and evaluate preliminary options for organizing the exterior form and interior spaces of a building. An example study suggests that thin-shell structures of minimum weight, and even timber buildings, may be optimally tuned to produce ample ventilation and temperature attenuation.

6 **Keywords:** Thermal mass, Natural ventilation, Thermal Resilience, Materials design, Life Cycle  
7 Analysis, Thermal optimization, Low carbon

---

8 **1. Introduction**

9 What proportions should a thermally massive building have? How should the thermal mass be  
10 distributed? Should the "massing" change with the choice of material? Recent studies on termite  
11 air-conditioning—the outside temperature, swinging up and down, thermally activates the mound,  
12 powering the ventilation—suggest we still have much to learn [1–4].

---

\*Corresponding author.

Email address: [salmaan.craig@mcgill.ca](mailto:salmaan.craig@mcgill.ca) (Salmaan Craig)

13 Builders have intuitively harnessed the heat storage capacity of stone, brick, and earth for mil-  
14 lennia [5–7]. Since the middle of the 20th century, engineers have used mathematical analysis and  
15 computer models to simulate the dynamics of thermal mass [6, 8–11]. In the last three decades, build-  
16 ing scientists have made increasingly accurate descriptions of temperature-driven ventilation, such as  
17 what happens when buoyant airflow and thermal mass are bound together by the ambient temperature  
18 swing in a natural feedback loop [12, 13]. How to synchronize these ambient heat exchanges is the  
19 focus of this paper. The analysis shows how to make optimal adjustments to the form, height, mass,  
20 and openings of a building, based on ratios that balance the accumulation of heat inside the mass with  
21 its later release by thermal venting.

22 Thermal mass is widely recognized as an opportunity for greater material integration between  
23 structural and thermal design [14]. In the next decade, building design teams may be forced to shrink  
24 and simplify the material inventories of their design proposals to meet strict limits on greenhouse gas  
25 emissions [15–17]. As well as using construction materials in smaller quantities and for longer lifetimes,  
26 the emphasis will be on finding intelligent ways of organizing, shaping, and upgrading these materials,  
27 so that ancillary building products and artificial climate control are less needed, and renovation, reuse,  
28 and recycling are more straightforward in later life-stages [18, 19]. The method outlined in this paper is  
29 meant to help design teams achieve this kind of material integration—within carbon limits and without  
30 sacrificing the physical and spatial qualities of the architecture, or overdetermining its possible uses in  
31 an uncertain future.

32 It may be some time before the industry establishes a consensus on how to accurately account  
33 for the carbon-dioxide emissions associated with construction. Efforts are underway to improve the  
34 quality of emissions data, make them widely and freely available, and to standardize the accounting  
35 and reporting procedures [20–22]. However, as one study recently highlighted [23], the discrepancy  
36 between results from different carbon accounting methods can be significant—larger, even, than the  
37 savings either method estimates for alternative design schemes. This scale of uncertainty is disabling  
38 for decision-makers. It seems to propagate in proportion to the number of components: the more  
39 complex the material assembly, the more difficult it is to get an accurate picture of the potential web  
40 of ecological upheaval. Reducing the material intensity of buildings could, therefore, result in a double  
41 dividend: real reductions in carbon-dioxide emissions, and more reliable predictions of these reductions.

42 In the construction industry, the materials supply chain is decentralized, and technical knowledge  
43 is distributed among independent, competing organizations [24]. At any moment in this complex and

44 unpredictable web of social relations (Figure 1), technical expertise is liable to fragment, forcing the  
 45 piecemeal resolution of technical concerns. Opportunities for integration across functional systems slip  
 46 by the wayside (Figure 2 ), increasing the complexity of the materials inventory. Engineering models  
 47 must do their work against the background of this shared context. The results of a model can help to  
 48 establish consensus and steer the activities of other project contributors and stakeholders. In the early  
 49 stages of design, architects develop a range of volumetric forms to facilitate discussion with project  
 50 contributors and stakeholders. These so-called "massing studies" do not need to be geometrically  
 51 detailed; their purpose is to help build consensus on which issues and ideas to prioritize and develop  
 52 further.

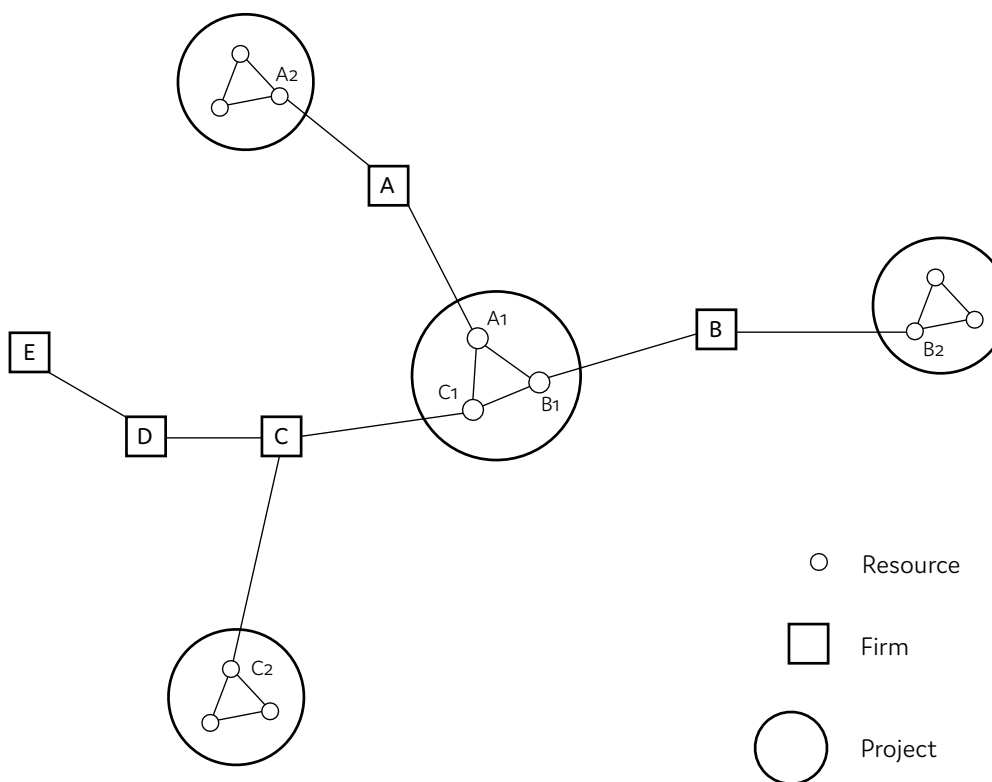


Figure 1: A construction project in its dynamic, social context (adapted from [24]). Firms A, B, and C have different expertise. They must balance their resources competitively and simultaneously across several projects. Technical knowledge is therefore distributed among loosely coupled communities. It can be organized according to any project but is liable to fragment if social relations weaken or breakdown.

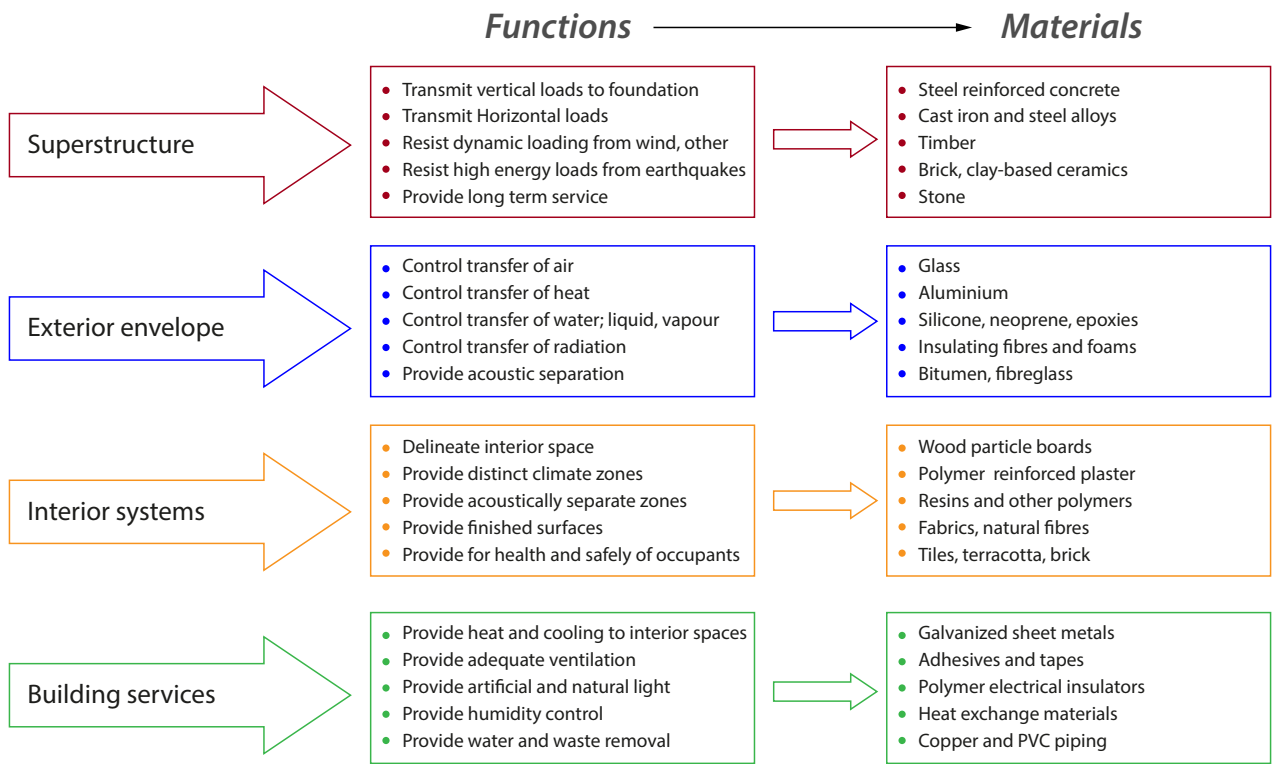


Figure 2: The functional systems of a modern building (adapted from [25]). Dividing up functions in this way helps to organize the expertise and activities of project contributors. But it can also mask opportunities for functional integration, and wastefully increase the size and scope of the materials inventory.

53 The parameters and ratios [26] presented in this paper can be used as a *strategic model* for thermal  
 54 and material massing. The model is meant to help design teams [27, 28] produce and compare options  
 55 in the preliminary stages, improving their ability to integrate technical systems and understand the  
 56 associated environmental impacts. The ratios and parameters are not suitable as a *forecasting model*,  
 57 i.e. to estimate future patterns of energy use and thermal comfort in absolute terms. Forecasting  
 58 models require detailed input information: their prediction quality improves as design decisions settle  
 59 and finalize. In contrast, a strategic model must establish what constitutes a well-performing design  
 60 and show what the requisite balance of technical parameters are—but without predetermining the  
 61 final design configuration. Strategic models are most effective when they are stripped down to their

62 essential relations so that the causal workings are transparent to all members of the project team and  
63 everyone can agree that the model is a suitable proxy for reality.

64 Experienced analysts may use a strategic model to frame the parameters of debate. For instance,  
65 they may treat the model as an opportunity to inform project stakeholders on recent research in  
66 adaptive comfort [29–43], advocating for natural ventilation principles to be incorporated into the  
67 schematic design. In such a case, the analyst may try to show the cumulative influence of passive  
68 design measures on the floating or free-running temperature; that is, how the interior temperature  
69 evolves without active thermostatic control. With the frequency and intensity of heatwaves increasing  
70 all over the world [44–46], the free-running temperature provides a basis for sizing cooling plants [47–49]  
71 but also indicates whether interior conditions will stay safely within physiological limits for heat-stress,  
72 particularly when there is a blackout or when occupants cannot afford to run or install mechanical  
73 cooling. Comparing the free-running temperature to thresholds for adaptive comfort and dangerous  
74 heat-stress can, therefore, indicate the thermal resilience of a proposed design [50–53].

75 Here is an example of one possible calculation flow using the method presented in subsequent  
76 sections. The design team decides on the free-running temperature (relative to the exterior swing of  
77 temperature), the rate of buoyancy ventilation (to satisfy the needs of occupants and their activities),  
78 the thermal massing material (which may serve a structural function, too), and the notional height  
79 of the building (which co-determines the potential energy for driving the buoyancy ventilation). The  
80 equations then give the optimum thickness and surface area of that material (operating as externally  
81 insulated thermal mass) and the necessary size of ventilation openings (i.e. the effective open area).  
82 The team can then evaluate a range of options that achieve the same performance but with different  
83 geometries and massing materials (and repeat the process with different inputs as necessary).

## 84 2. Previous work

85 Thermal mass refers to the ancient practice of configuring spaces and materials so that the materials  
86 passively store heat during the day then release it at night; as a result, the interior stays naturally  
87 cool in the hottest parts of the day [54–58]. Where to place thermal mass in the building envelope—  
88 The innermost layer? The outermost layer? Both?—is a recent concern. Modern life is increasingly  
89 spent indoors with technological accouterments that generate extra heat, while building envelopes are  
90 now composed of several material layers, each with specific functions to accommodate the need for  
91 insulation and air-tightness. The most direct way to absorb excess heat generated by interior activities

92 is to expose the mass on the innermost layer (i.e. so it is an "internal mass"). External insulation  
93 and shading then protect the mass from ambient heat and baking sunshine. However, the absorbed  
94 interior heat must somehow be discharged at night for the cooling effect to work the following day.  
95 This discharging can be done by ventilation.

96 Buoyancy ventilation, otherwise known as stack ventilation, refers to the practice of configuring  
97 spaces and openings so that the airflow is driven spontaneously by the temperature difference between  
98 inside and outside. In updraft mode, warm air rises and escapes out the top while cooler air floods  
99 in from below to replace the evacuating air. In downdraft mode, the cycle reverses: cooler air spills  
100 out from below and warmer air floods in from above. In recent years, there have been major advances  
101 in the engineering theory of buoyancy ventilation, otherwise known as the art of "emptying a filling  
102 box" [59–62]. Researchers have solved problems such as how to keep the emptying air from stratifying  
103 to save energy on colder days [63, 64], how to differentially size openings in a multistorey building  
104 according to the vertical pressure gradient [65, 66], and how the cooling from thermal mass or another  
105 source changes the flow to a downdraft [67–70]

106 Unlike stochastic wind forces, buoyancy forces can be balanced and harnessed in a stable and  
107 continuous feedback loop. Sustaining this loop in temperate weather is straightforward. Demand for  
108 ventilation exists when people are present: these people and their activities generate heat; this heat  
109 can power the ventilation; therefore, balance the temperature and flow rate by sizing the stack and  
110 adjusting the openings accordingly. The balancing act is not quite so simple in hot weather. Some  
111 cooling is needed to cancel the heat loads and to keep the interior below ambient temperature. Most  
112 or all of this cooling can come from thermal mass—so long as the ventilation and heat storage cycles  
113 are well synchronized.

### 114 2.1. Coupling mass and buoyancy

115 In 2003, Yam, Li, and Zheng [71] were the first to examine the non-linear coupling between an  
116 internal thermal mass and buoyancy ventilation. Yam *et al.* derived differential equations to describe  
117 this non-linear behavior and solved them numerically. The results showed a close-to-periodic variation  
118 of the interior temperature. This finding led them to conclude that harmonic analysis could reasonably  
119 represent the coupling, assuming an average heat transfer coefficient for the surface.

120 Inspired by this finding, Holford and Woods [12] undertook a thorough mathematical investigation  
121 of the coupling in 2007. They parameterized the relationships between diffusion through an internal  
122 mass, convection at its surface, and buoyancy ventilation, and described the relationships in terms of

123 dimensionless ratios. They then solved the differential equations numerically for a range of scenarios,  
 124 assuming periodic (i.e. harmonic) variations in the ambient temperature. Using the same parameters,  
 125 they then built an approximate lumped model, and systematically compared the results of this approx-  
 126 imate model to the more detailed numerical version—and found good agreement. Significantly, their  
 127 lumped model is discretized into four interacting temperature signals—the exterior temperature, the  
 128 interior temperature, the surface temperature of the internal mass, and the lumped temperature of the  
 129 mass (Figure 3). The ability to accurately estimate the coupled surface and interior temperature—using  
 130 analytical shortcuts—represented a significant advance in the thermal mass literature.

2

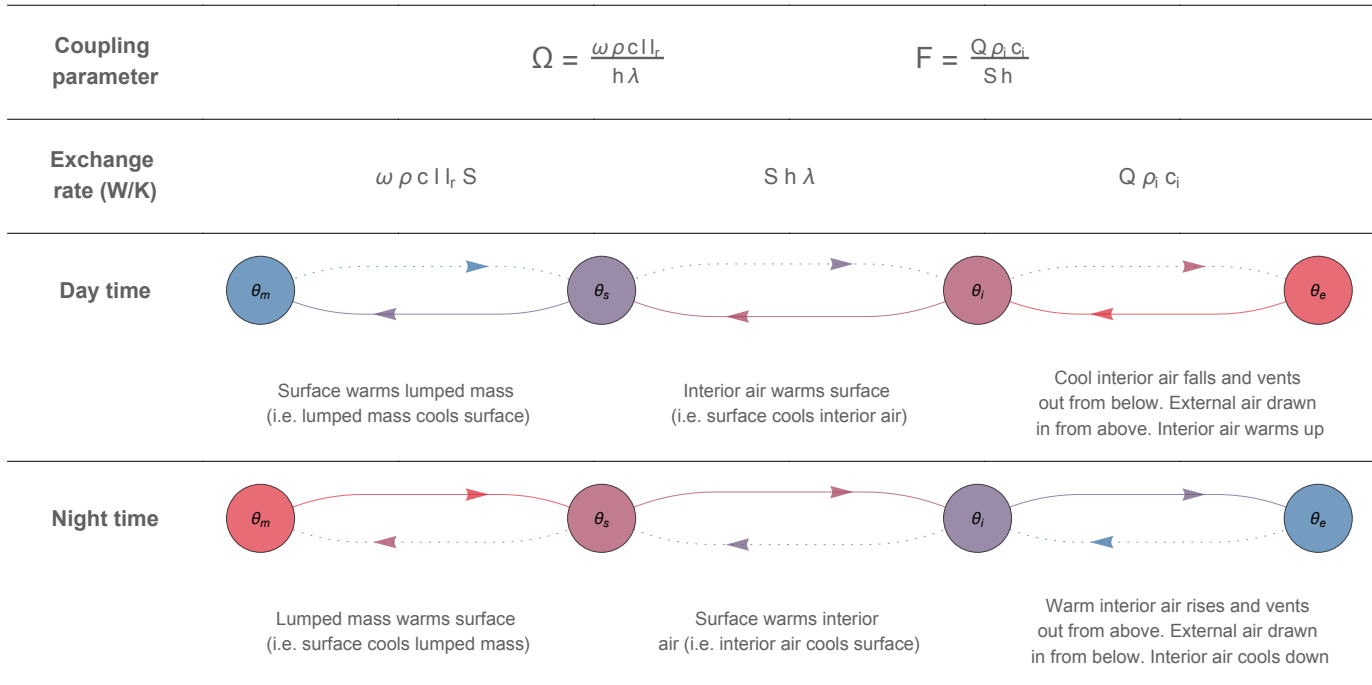


Figure 3: The natural feedback loop between internal thermal mass and buoyancy ventilation, as parameterized by Holford & Woods [12]

131 In 2008, unaware of the work of Holford and Woods, Zhou *et al.* [72] added to the work of Yam *et*  
 132 *al.* (Li was a common co-author) by outlining a method to solve for the interior surface temperature,  
 133 based on harmonic analysis. Their approach also considered periodic losses and gains from exterior  
 134 insulation (both Yam *et al.* and Holford and Woods had assumed adiabatic boundary conditions, i.e.  
 135 perfect insulation). In 2011, interested in the effects of massive floors, ceilings, and furniture, Zhou *et*  
 136 *al.* [73] showed how to bundle the buffering effects of different pieces of thermal mass into a 'virtual  
 137 sphere', posing the question: why relegate thermal mass to the envelope at all?

138 In 2009, Lishman and Woods [13] characterized thresholds for how natural ventilation behaves in  
139 thermally massive buildings. These thresholds depend on the unsteady balance between buoyancy  
140 forces, wind forces, interior heating, and heat storage. They found that the balance of these forces  
141 plays out on short and long time-scales, making for a surprising range of possible evolutionary paths  
142 and final flow regimes. For instance, if the interior heat load suddenly changes, the regime may rapidly  
143 switch from wind-driven to buoyancy-driven flow, only to switch back hours later once the thermal  
144 mass adjusts to the changes. Understanding these path-dependencies is important, so that they can  
145 be strategically avoided or harnessed by design.

146 In 2012, unaware of the work of Lishman and Woods (but citing other important works, e.g. [74–  
147 76]), Faure and Roux [77] analyzed the short and long term effects that thermal mass has on natural  
148 displacement ventilation, focusing on features such as the stratification height and how this inter-  
149 face buoys or "overshoots" before settling to steady-state. In 2016, Yang and Guo [78] analyzed the  
150 coupling between internal mass and buoyancy ventilation using Fourier components at multiple fre-  
151 quencies, to understand the temperature evolution of the system when driven by more realistic ambient  
152 conditions—that is, an exterior temperature signal which is not quite sinusoidal. Comparing their pre-  
153 dictions to data from a small physical experiment, they confirmed that these more realistic excitations  
154 produced ventilation flow rates that are *anharmonic* (but which are nevertheless predictable with  
155 Fourier analysis).

156 In 2018, Bastien and Athienitis [79, 80] gave a skilled demonstration of how to design thermal  
157 mass inside greenhouses and solaria. They did some parametric design studies using the frequency  
158 response method (combining Laplace transforms and Fourier analysis), then followed this up with  
159 detailed annual simulations using the finite-difference method. The parametric studies allowed them  
160 to compare different approaches to optimizing the thermal mass thickness, arguing that the best  
161 approach for solaria was to control the delay between when the mass absorbs most sunshine and when  
162 it releases this heat.

163 Lots of research has been published in the thermal mass literature since the turn of the century,  
164 especially for efficient methods to simulate thermal mass in arbitrary configurations [9, 10, 81–89].  
165 However, it seems that very little of this new knowledge has been distilled into design parameters and  
166 ratios to help architects and planners to proportion thermal mass buildings properly—particularly in  
167 light of the material integration and cooling challenges posed by climate change. Of all the studies  
168 on thermal mass, the work by Holford and Woods seems to be the most promising as a basis for the

169 necessary design guidance.

170 *2.2. The Holford and Woods model*

171 Figure 3 describes the feedback loop between thermal mass and buoyancy ventilation, as modelled  
 172 and parameterized by Holford and Woods [12]. The parameters  $F$  and  $\Omega$  are dimensionless numbers  
 173 (i.e. they are ratios without units). They control the relative heat exchange between ventilation and  
 174 thermal mass, respectively. When  $F \sim \Omega \sim 1$ , the heat exchange between the ventilation and the  
 175 thermal mass is balanced. When  $\Omega \gg F$ , the thermal mass dominates—the interior temperature is  
 176 highly damped, and the air changes are relatively low. When  $F \gg \Omega$ , the ventilation dominates—the  
 177 air changes are relatively high, and the thermal mass hardly affects the interior temperature.

178 The two ends of the causal chain in Figure 3 are unconnected, and this highlights one of the most  
 179 significant simplifications in the Holford and Woods model. The model assumes an internal mass,  
 180 meaning there is no heat transfer at the outer face. There mass is *indirectly* connected to the external  
 181 environment, via the interior air. These adiabatic boundary conditions are equivalent to perfect exterior  
 182 insulation, or adjacent spaces with perfectly replicated thermal conditions.

183 Figure 4 shows the influence of  $F$  and  $\Omega$  on the interior, surface, and mass temperatures during  
 184 a 24-hour cycle. The temperature signals are normalized, so they are relative to maximum 1 and  
 185 minimum -1 while the time is expressed in radians. The outside temperature varies periodically:

$$T_e(t) = T_0 + \Delta T \cos(\omega t) \quad (2.1)$$

186 Where  $T_0$  is the mean daily temperature,  $T_0 = (T_{min} - T_{max})/2$ ,  $\Delta T$  is the temperature increment  
 187 above the mean,  $\Delta T = |T_{max} - T_0|$ , and  $\omega$  is the angular frequency,  $\omega = 2\pi/86400$ . The dimensionless  
 188 time and temperature are, respectively:

$$\tau = \omega t \quad (2.2)$$

$$\theta = \frac{(T - T_0)}{\Delta T} \quad (2.3)$$

189 The four temperatures in the system are defined as follows. The exterior temperature:

$$\theta_e = \cos(\tau) \quad (2.4)$$

190 The interior temperature (assuming perfectly mixed air):

$$\theta_i = \frac{\cos(\tau - \Phi_i)}{A_i} \quad (2.5)$$

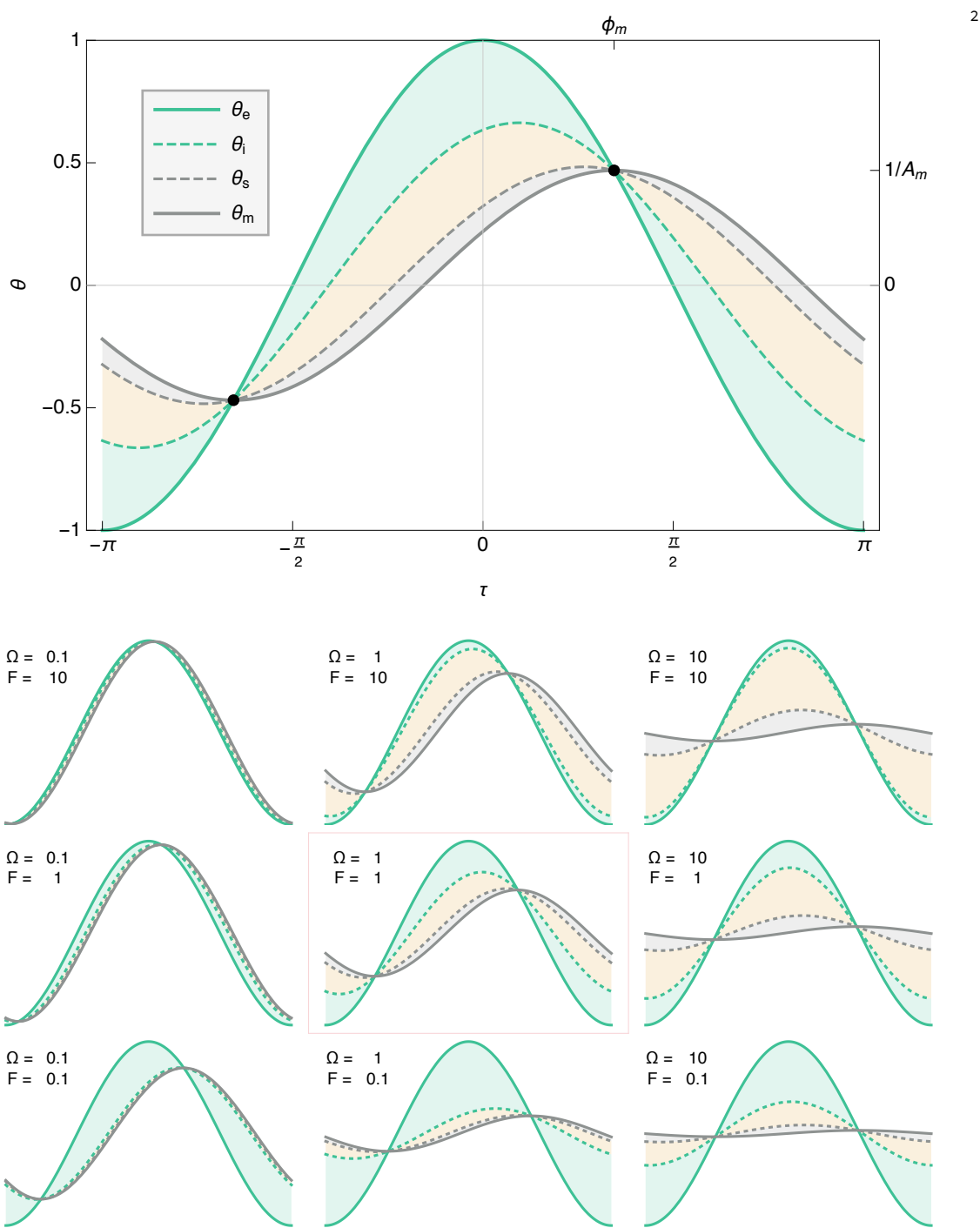


Figure 4: The influence of the ventilation parameter  $F$  and the massing parameter  $\Omega$  on the relative floating temperatures,  $\theta_i$ ,  $\theta_s$ ,  $\theta_m$  (i.e. interior, surface, mass), driven by cyclic changes in the external temperature  $\theta_e$  over a period of  $2\pi = 24$  hours, after Holford & Woods [12]. The surface temperature delay of the thermal mass is arbitrarily fixed at  $\lambda = 0.75$  in all graphs.

191 The surface of the thermal mass facing the interior:

$$\theta_s = \frac{\cos(\tau - \Phi_s)}{A_s} \quad (2.6)$$

192 And the temperature of the thermal mass:

$$\theta_m = \frac{\cos(\tau - \Phi_m)}{A_m} \quad (2.7)$$

193 The thermal mass is modelled as a lumped mass, meaning that, unlike a real mass, there are no  
 194 temperature gradients inside it. A lumped mass has a single evolving temperature that represents the  
 195 equivalent work of a real mass. The lumped mass temperature signal is close to, but not the same as,  
 196 the average temperature of a real mass.

197 To plot the temperature signals, one needs to know the attenuation ( $A$ ) and the phase lag ( $\Phi$ ). The  
 198 reciprocal of the attenuation ( $1/A$ ) is the peak temperature, relative to  $\theta_e = 1$ . The phase lag is the  
 199 time delay of the peak temperature, relative to  $\tau = 0$ . The attenuation for the interior temperature  
 200 is:

$$A_i = \frac{A_m}{\sqrt{1 + \Omega^2}} \quad (2.8)$$

201 The attenuation for the surface temperature is:

$$A_s = \frac{A_m}{\sqrt{1 + \Omega^2(1 - \lambda)^2}} \quad (2.9)$$

202 And the attenuation for the mass temperature is:

$$A_m = \frac{1}{\cos(\Phi_m)} \quad (2.10)$$

203 The parameters  $\lambda$  and  $\Omega$  will be defined shortly. The phase lag of the interior temperature is:

$$\Phi_i = \Phi_m - \tan^{-1}(\Omega) \quad (2.11)$$

204 The phase lag of the surface temperature is:

$$\Phi_s = \Phi_m - \tan^{-1}((1 - \lambda)\Omega) \quad (2.12)$$

205 Algebraic substitution reveals that the temperature definitions all include  $\Phi_m$ :

$$\theta_i = \sqrt{1 + \Omega^2} \cos(\Phi_m) \cos(\tau - \Phi_m + \tan^{-1}(\Omega)) \quad (2.13)$$

$$\theta_s = \sqrt{1 + (1 - \lambda)^2 \Omega^2} \cos(\Phi_m) \cos(\tau - \Phi_m + \tan^{-1}((1 - \lambda)\Omega)) \quad (2.14)$$

$$\theta_m = \cos(\Phi_m) \cos(\tau - \Phi_m) \quad (2.15)$$

206 How to solve for the mass phase lag,  $\Phi_m$ ? The first option is to numerically solve the differential  
 207 equations that define their lumped parameter model:

$$\begin{aligned} \Omega \frac{d\theta}{d\tau} &= \theta_i - \theta_m \\ 0 &= \lambda(\theta_m - \theta_i) + F(\theta_e - \theta_i) |\theta_e - \theta_i|^{1/2} \end{aligned} \quad (2.16)$$

208 Alternatively, Holford and Woods found two shortcuts for estimating  $\Phi_m$ :

$$\left( \frac{\tan(\Phi_m)}{\Omega} - 1 \right)^6 = \left( \frac{\lambda^2}{\Omega F^2} \right)^2 \left( 1 + \frac{1}{\Omega^2} \right) (1 + \tan^2(\Phi_m)) \quad (2.17)$$

$$\frac{\tan(\Phi_m)}{\Omega} = 1 + 1.07 \left( \frac{\lambda^2}{\Omega F^2} \right)^{1/3} \quad (2.18)$$

209 They compared the accuracy of Equation (2.16), Equation (2.17), and Equation (2.18) against a full  
 210 numerical model (which represented diffusion through the mass with finite-differences and which al-  
 211 lowed the ventilation to vary non-linearly). They found that Equation (2.16) and Equation (2.17) stay  
 212 accurate to within 0.1% and 1%, respectively, across parameter space—even for very extreme scenarios  
 213 (e.g. when a very thick mass combines with a very high rate of ventilation, leading the surface temper-  
 214 ature to stray far from the mass temperature). Equation (2.18) is less consistent; it is only reasonably  
 215 accurate for balanced scenarios.

216 Since  $\Phi_m$  is determined by parameters  $\Omega$ ,  $\lambda$ , and  $F$ , these three parameters alone control the entire  
 217 system. The massing parameter  $\Omega$  is defined as:

$$\Omega = \frac{\xi(\cosh(2\eta) - \cos(2\eta)) + \eta(\sinh(\eta) - \sin(2\eta))}{\eta(\sinh(2\eta) + \sin(2\eta))} \quad (2.19)$$

218 Where  $\xi$  is the potential rate of heat storage compared to the rate of surface heat transfer:

$$\xi = \frac{\omega \rho c l}{h} \quad (2.20)$$

219 And  $l$  is the thickness of the mass,  $\rho c$  is the volumetric heat capacity of the mass material, and  $h$  is  
 220 the surface heat transfer coefficient. The parameter  $\eta$  is the ratio of the layer thickness to the depth  
 221 of thermal penetration :

$$\eta = l \sqrt{\frac{\omega}{2\alpha}} \quad (2.21)$$

222 Where  $\alpha$  is the thermal diffusivity of the mass material. The massing parameter can also be written  
 223 as:

$$\Omega = \frac{\xi l_r}{\lambda} = \frac{\omega \rho c l l_r}{h \lambda} \quad (2.22)$$

224 Where  $l_r$  is the fraction of material thickness needed for the lumped mass to do the equivalent work of  
 225 the real mass:

$$l_r = \frac{(\cosh(2\eta) - \cos(2\eta))}{\eta (\sinh(2\eta) + \sin(2\eta))} \quad (2.23)$$

226 And  $\lambda$  is a factor which, by approximating the temperature gradients inside the mass, determines the  
 227 surface temperature:

$$\lambda = \frac{1}{1 + \frac{\eta (\sinh(2\eta) - \sin(2\eta))}{\xi (\cosh(2\eta) - \cos(2\eta))}} \quad (2.24)$$

228 This surface temperature factor ranges between  $0 < \lambda < 1$ . When  $\lambda = 1$ , there are no temperature  
 229 gradients inside the mass, so  $\theta_s = \theta_m$ . When  $\lambda \rightarrow 0$ , the surface temperature strays further and further  
 230 away from the mass temperature; as a result, the mass stores heat less and less efficiently.

231 Finally, we can define the ventilation heat exchange parameter, which compares the ventilation  
 232 heat exchange to the surface heat exchange at the surface:

$$F = \frac{Q \rho_i c_i}{S h} \quad (2.25)$$

233 Where  $\rho_i c_i$  is the volumetric heat capacity of air,  $S$  is the surface area of mass exposed to the interior  
 234 air, and the rate of ventilation,  $Q$ , is:

$$Q = A^* \sqrt{\beta g H |T_e - T_i|} \quad (2.26)$$

235 Where  $A^*$  is the effective area of ventilation openings (see [90]),  $\beta$  is the thermal expansion coefficient of  
 236 air, and  $H$  is the stack height. The rate of ventilation, powered by buoyancy, depends on the interior  
 237 temperature—which in turn depends on the rate of ventilation (c.f Figure 3). Holford and Woods  
 238 suggest setting  $|T_e - T_i| = \Delta T$  in Equation (2.26) to obtain a reference ventilation rate. Alternatively,  
 239 we define an average ventilation rate, based on the normalized mean temperature difference:

$$Q = A^* \sqrt{\beta g H \Delta T |\theta_e - \theta_i|_{mean}} \quad (2.27)$$

240 According to the integral mean value theorem, the mean temperature difference is:

$$|\theta_e - \theta_i|_{mean} = \frac{1}{b - a} \int_a^b |\theta_e - \theta_i| d\tau \quad (2.28)$$

241 Where  $b = \Phi_m - \pi$  and  $a = \Phi_m$  mark the beginning and end of half a cycle. Substituting equations  
 242 Equation (2.4) and Equation (2.13) and completing the integration gives:

$$|\theta_e - \theta_i|_{mean} = \frac{-2 \Omega \cos(\Phi_m) + 2 \sin(\Phi_m)}{\pi} \quad (2.29)$$

243 **3. Analysis**

244 §2 identified the work of Holford and Woods [12] as a promising basis for design guidance on how  
 245 to proportion thermally-massive buildings. Using their parameterization, this section finds a new way  
 246 to optimally synchronize the coupling of internal thermal mass and buoyancy ventilation.

247 *3.1. The optimal tuning*

248 The Holford and Woods model (c.f. §2.2) describes the coupling between internal thermal mass  
 249 and buoyancy ventilation. This coupling is controlled by two non-dimensional parameters:  $F/\lambda$  (the  
 250 ratio of ventilation heat transfer to surface heat transfer) and  $\Omega$  (the ratio of thermal storage to surface  
 251 heat transfer). This section defines two optimal tunings for  $F/\lambda$  and  $\Omega$ . The two optimal tunings are  
 252 associated with different damping coefficients, defined graphically in Figure 5

253 The first damping coefficient is the maximum difference between the interior and exterior temper-  
 254 ature in a given cycle,  $|\theta_e - \theta_i|_{peak}$ . Let us call it the *peak venting temperature difference*, since it is  
 255 the moment of maximum buoyancy ventilation. It occurs twice in a 24-hour cycle, but when exactly?  
 256 As indicated in figures 4 and 5, all temperatures in the system converge at time  $\tau = \Phi_m$ . When  
 257 this happens, the buoyancy ventilation momentarily ceases before switching direction from a daytime  
 258 downdraft to a nocturnal updraft. If the minimum venting temperature difference occurs at time  
 259  $\tau = \Phi_m$ , it follows that the peak venting temperature difference occurs midway through a half-cycle  
 260 at time  $\tau = \Phi_m - \pi/2$ . Subtracting equation 2.12 from 2.4 and substituting the definition for  $\tau$  gives:

$$|\theta_e - \theta_i|_{peak} = -\Omega \cos(\Phi_m) + \sin(\Phi_m) \quad (3.1)$$

261 Now is necessary to substitute a definition for  $\Phi_m$ . As discussed in §2.3, Equation (2.18) is less ac-  
 262 curate than Equation (2.17), but it does have the advantage of not needing to be solved iteratively.  
 263 Moreover, recall from §1 that strategic comparisons, not absolute forecasts, are the focus of this paper.  
 264 Substituting Equation (2.18) gives:

$$|\theta_e - \theta_i|_{peak} = \frac{1.07 \left( \frac{\lambda^2}{F^2 \Omega} \right)^{1/3} \Omega}{\sqrt{1 + \left( \Omega + 1.07 \left( \frac{\lambda^2}{F^2 \Omega} \right)^{1/3} \Omega \right)^2}} \quad (3.2)$$

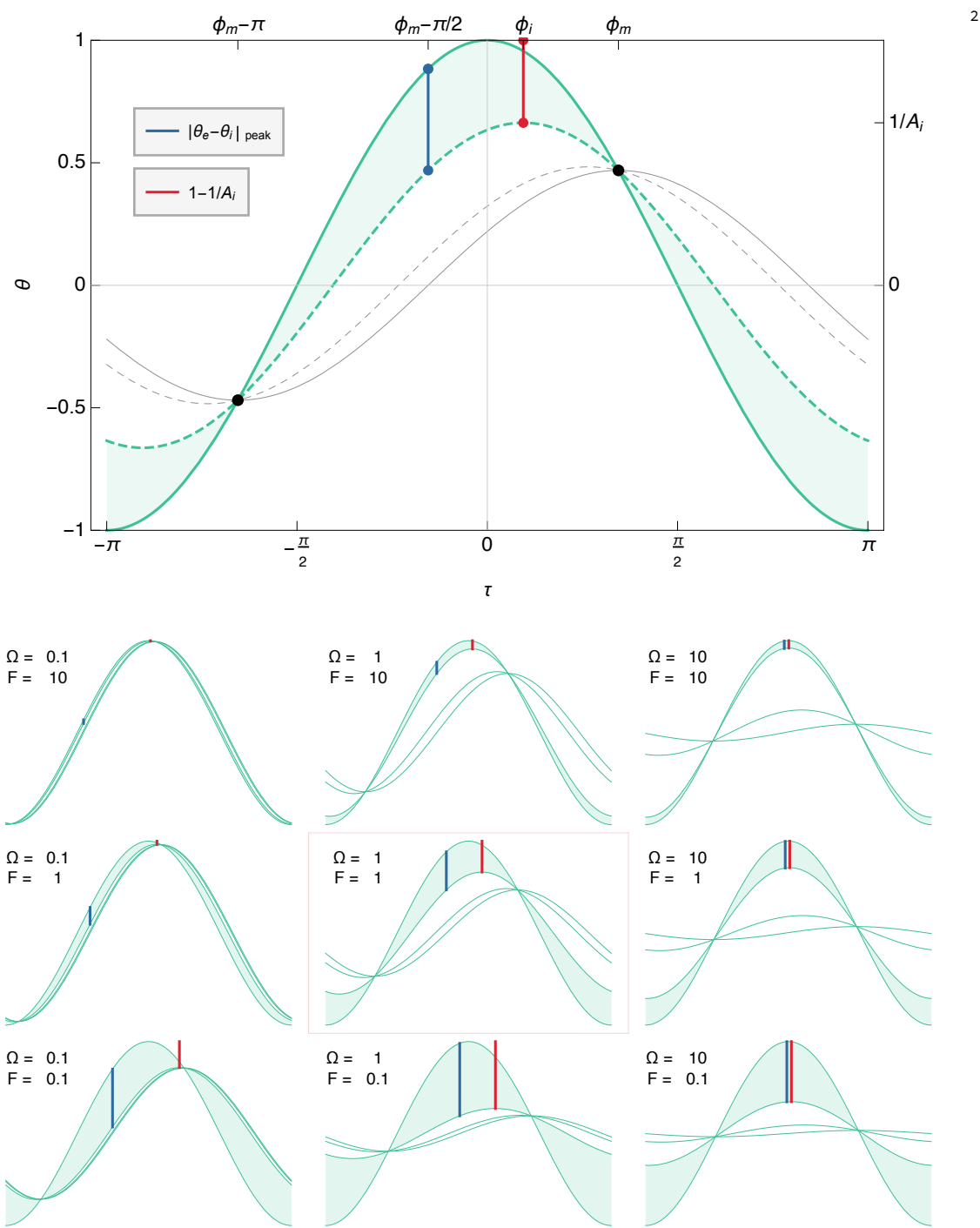


Figure 5: The definition of two damping coefficients: the peak venting temperature difference, which is shown in blue and occurs at time  $\tau = \Phi_m - \pi/2$ , and the attenuating temperature difference,  $1 - 1/A_i$ , which is shown in red and occurs at time  $\tau = \Phi_i$ . The graphs show the influence of  $F$  and  $\Omega$  on both kinds of damping coefficient. The surface temperature delay of the thermal mass is arbitrarily fixed at  $\lambda = 0.75$  in all graphs.

265 Figure 6 shows a contour plot of the peak venting temperature difference as a function of  $F/\lambda$  and  $\Omega$ .  
 266 Notice how, for every increment of  $|\theta_e - \theta_i|_{peak}$ , there is an optimal pairing of  $\Omega$  and  $F/\lambda$ . This ideal  
 267 tuning is defined by the curve:

$$(F/\lambda)_{max} = \sec(1.07\Omega^{4/3}) - 1 \quad (3.3)$$

268 Optimal design values can be found by solving Equation (3.2) and Equation (3.3) simultaneously. To  
 269 do this, one needs to consider  $F/\lambda$  as a single variable in Equation (3.2) (i.e. so that  $\left(\frac{\lambda^2}{F^2\Omega}\right) = \left(\frac{1}{a^2\Omega}\right)$ ,  
 270 where  $a = F/\lambda$ ). The independent values for  $F$  and  $\lambda$  can be found later. For instance, solving  
 271 Equation (3.2) and Equation (3.3) tells us that to optimize for  $|\theta_e - \theta_i|_{peak} = 0.5$ , one should design  
 272 the thermal mass such that  $\Omega = 0.94$ ; this will maximize the  $F/\lambda$  parameter such that  $F/\lambda = 0.83$ .  
 273 Now recall that  $\lambda$  predicts the surface temperature delay due to temperature gradients inside the mass,  
 274 and depends on the choice of the material. If calculations for one material show that  $\lambda = 0.9$ , then  $F$   
 275 =  $0.83 * 0.9 = 0.747$  (see §4.1 for a more detailed example).

276 In this way, one can evaluate the effect of the thermal properties of materials fairly. All material  
 277 masses can be sized to achieve the same optimal value for the massing parameter  $\Omega$ —it is just a matter  
 278 of finding the correct thickness. However, because of differences in thermal properties, different material  
 279 masses can't have the same values for both  $\Omega$  and  $\lambda$ . The differences in  $\lambda$  manifest as differences  
 280 in surface temperature, and the surface temperature regulates the power of buoyancy ventilation.  
 281 Therefore, everything else being equal, materials with a lower  $\lambda$  are less efficient as thermal mass  
 282 because *they produce less ventilation*.

283 Figure 5 defines a second damping coefficient, which occurs at time  $\tau = \Phi_i$ . Let us call it the  
 284 *attenuating temperature difference*:

$$1 - \frac{1}{A_i} = 1 - \sqrt{1 + \Omega^2} \cos(\Phi_m) \quad (3.4)$$

285 Substituting equation 2.11 gives:

$$1 - \frac{1}{A_i} = 1 - \frac{\sqrt{1 + \Omega^2}}{\sqrt{1 + \left(\Omega + 1.07 \left(\frac{\lambda^2}{F^2\Omega}\right)^{1/3}\Omega\right)^2}} \quad (3.5)$$

286 Figure 7 shows a contour plot of the attenuating temperature difference as a function of  $F/\lambda$  and  $\Omega$ .  
 287 Once more, notice how, for every temperature increment, there is an optimal value of  $\Omega$  for which  $F/\lambda$   
 288 is maximized. This ideal tuning is defined by the curve:

$$(F/\lambda)_{max} = \tan\left(\frac{1.07}{2}\Omega^{4/3}\right) - 1 \quad (3.6)$$

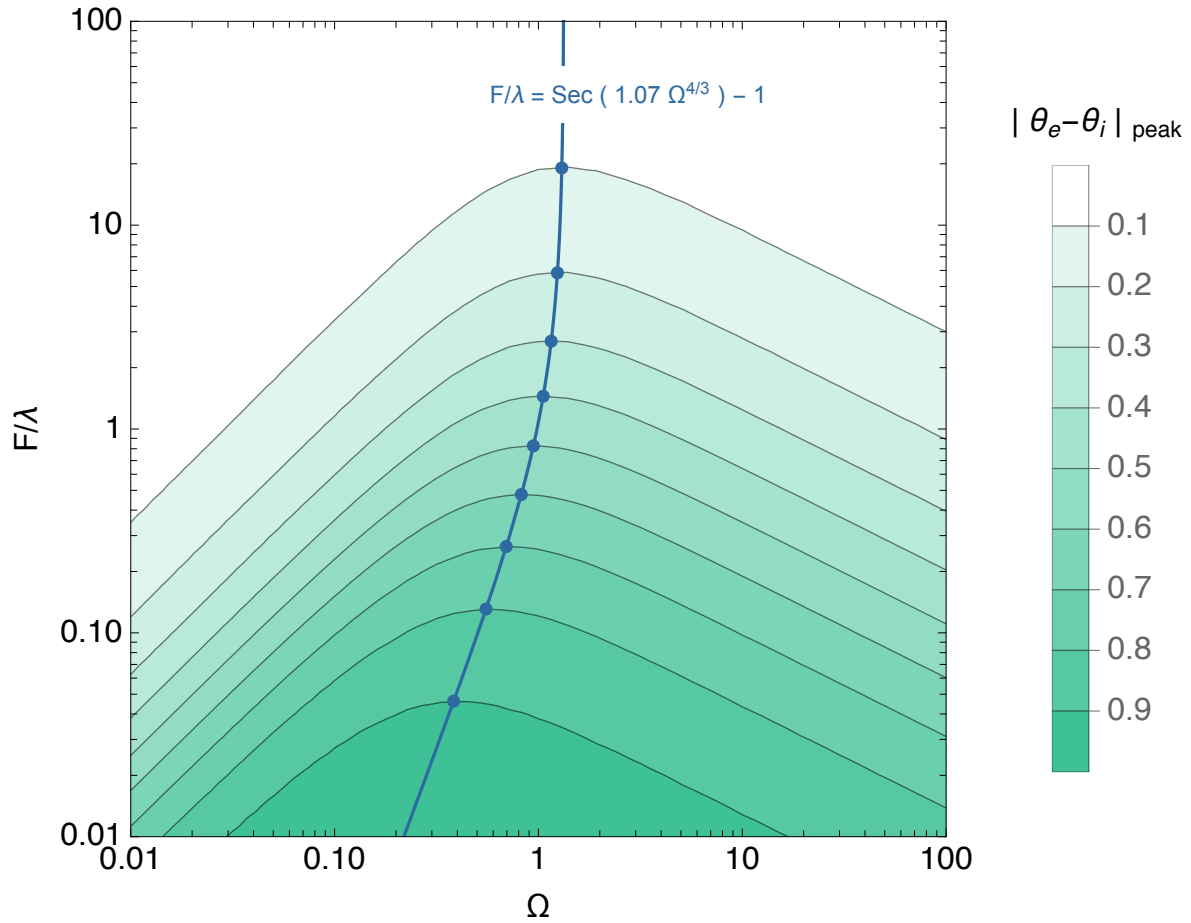


Figure 6: Contour plots of the peak venting temperature difference  $|\theta_e - \theta_i|_{peak}$ . The blue curve locates the optimal pairings of  $\Omega$  and  $F/\lambda$

Like before, optimal design values can be found by solving Equation (3.5) and Equation (3.6) simultaneously. For instance, to achieve  $1 - 1/A_i = 0.5$ , one should design the thermal mass such that  $\Omega = 1.62$ ; this will maximize the ventilation parameter such that  $F/\lambda = 0.61$ .

Notice that the optimal values for both damping coefficients are quite similar. The attenuating temperature difference is associated with slightly larger values for optimal  $\Omega$  and slightly smaller values for maximum  $F/\lambda$ . These small differences in the ideal tuning can have a large impact on the physical dimensions of the architecture, as the massing studies of §4 will show.

### 3.2. Surface heat transfer

The previous subsection described how to optimize thermal mass and natural ventilation in a feedback cycle, by finding ideal pairs  $F/\lambda$  and  $\Omega$  to synchronize the coupled heat exchanges. §4 explores the implications of these ideal proportions for sizing buildings and choosing materials. However, before doing this, a fair estimate of the surface heat transfer coefficient,  $h$ , is essential, as both  $F/\lambda$  and  $\Omega$

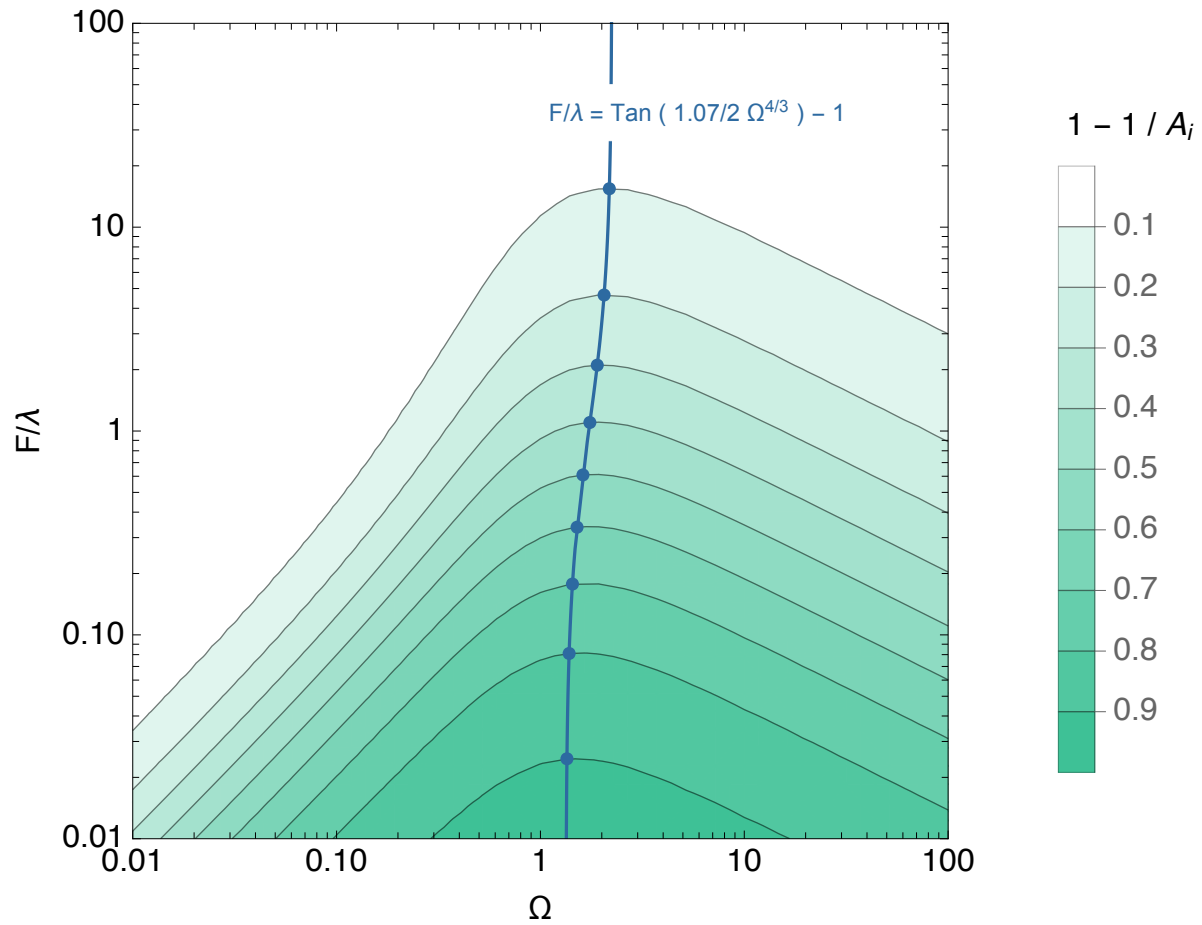


Figure 7: Contour plots of the attenuating temperature difference  $1 - 1/A_i$ . The blue curve locates the optimal pairings of  $\Omega$  and  $F/\lambda$

301 depend on it.

302 At the surface of an internal mass, sensible heat exchange occurs by convection and radiation.  
 303 The rate of convection determines the strength of coupling between the thermal mass and buoyancy  
 304 ventilation. Any radiation heat transfer has an indirect, but consequential, influence on this coupling.

305 Surface convection inside rooms can be driven naturally by surface temperatures, forcibly by nearby  
 306 air flows, or by a mixture of natural and forced convection. Forced convection on an interior surface  
 307 may be a consequence of breeze from fans, vents, and open windows, plumes from warm people and  
 308 equipment, or a larger circulation pattern powered by buoyancy inside the space. In this paper, natural  
 309 convection is the focus. Unlike forced convection, natural convection is guaranteed to happen in the  
 310 thermal feedback cycle described in this paper, and will do so in synchronization with the temperature  
 311 evolution of the system. If there is a particular scenario in which forced convection may be significant,  
 312 its influence on the baseline natural convection can be estimated by consulting the correlations in

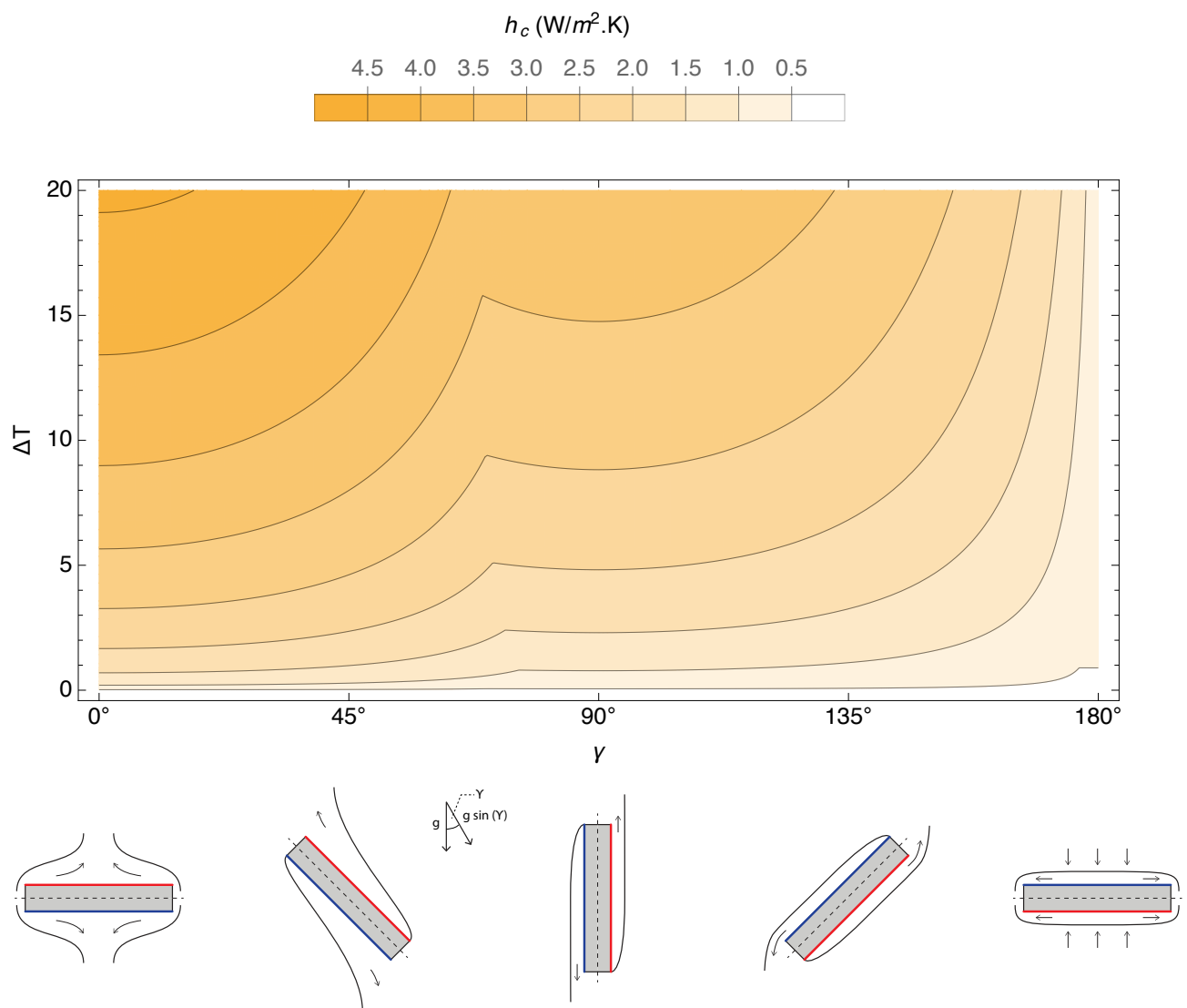


Figure 8: Contours of the average heat transfer coefficient,  $h$ , due to natural convection from a hot or cold surface. It varies according to the temperature difference, the rotation angle, and the size of the surface (here  $3 \times 3$  m).

313 the literature [91–93], or by running high-resolution transient simulations with computational fluid  
 314 dynamics incorporating the thermal energy equation [94].

315 The heat transfer coefficient for natural convection varies according to the interaction between thermal  
 316 and gravitational forces (Figure 8). The heat transfer coefficient is smallest when the orientation  
 317 of the surface ( $\gamma \rightarrow 180^\circ$ ) impedes warm air from rising or cool air from falling. In other orientations,  
 318 the heat transfer coefficient is larger. Turbulence ensues when viscous forces no longer dominate, and  
 319 the boundary layer de-laminates from the surface.

320 Figure 8 was computed using an algorithm recommended by Raithby and Hollands (see [95, 96]).

321 The algorithm evaluates five empirical correlations for the heat transfer coefficient: a pair of correlations  
 322 for surfaces at inclination  $\gamma = 0^\circ$  (one for laminar flow, one for turbulent flow); a pair for surfaces  
 323 at inclination  $\gamma = 90^\circ$  (laminar and turbulent); and one for surfaces at inclination  $\gamma = 180^\circ$  (gravity  
 324 keeps the flow practically quiescent in this case). For intermediate angles (e.g.  $\gamma = 77^\circ$ ), some other  
 325 equations combine results from two reference angles (e.g.  $\gamma = 0^\circ$  and  $\gamma = 90^\circ$ ) after balancing their  
 326 weights asymptotically. The five empirical correlations are not shown here. However, with some minor  
 327 exceptions, they all take the general form:

$$Nu = \frac{h_c k}{L} = m Ra^n \quad (3.7)$$

328 Where  $Nu$  is the Nusselt number,  $h_c$  is the average heat transfer coefficient for natural convection,  $k$   
 329 is the thermal conductivity of the fluid (in this case, air),  $L$  is the characteristic length of the surface  
 330 (e.g. the ratio of the area to the perimeter),  $n$  is a fraction less than 1 (usually  $1/4$  or  $1/3$ ),  $m$  is an  
 331 empirically derived constant, and  $Ra$  is the Rayleigh number:

$$Ra = \frac{g \beta L^3 (T_s - T_i)}{\nu \alpha} \quad (3.8)$$

332 Where  $\nu$  and  $\alpha$  are the viscosity and the thermal diffusivity of the air, respectively. While conducting  
 333 the calculations, the influence of the characteristic length ( $L$ ) was evidently weak for panel sizes bigger  
 334 than approximately 1 by 1 meter. Mathematically speaking, the weakening influence of  $L$  is because  
 335 the exponent  $n$  in Equation (3.7) asymptotically levels out the influence of the Rayleigh number (even  
 336 though  $Ra \propto L^3$ ). Physically speaking, air is not very viscous: on a large surface, the natural convec-  
 337 tion boundary layer soon reaches full turbulence, even if powered by a small temperature difference.  
 338 Therefore, Figure 8 (which assumes a surface of 3 by 3 meters) can be used to approximate the natural  
 339 heat transfer coefficient for many surface sizes inside rooms, at any inclination, from concrete table  
 340 tops to triple-height walls.

341 For an estimate of the *average* convection heat transfer coefficient, it is necessary to know the mean  
 342 temperature difference between the surface and the interior. According to the integral mean value  
 343 theorem:

$$|\theta_i - \theta_s|_{mean} = \frac{1}{b - a} \int_a^b |\theta_i - \theta_s| d\tau \quad (3.9)$$

344 Where  $b = \Phi_m - \pi$  and  $a = \Phi_m$  mark the beginning and end of half a cycle. Substituting equations  
 345 Equations (2.13) and (2.14) and completing the integration gives:

$$|\theta_i - \theta_s|_{mean} = \frac{2 \lambda \Omega \cos(\Phi_m)}{\pi} \quad (3.10)$$

346 The average surface heat flux can now be defined as:

$$q_{mean} = h \Delta T |\theta_s - \theta_i|_{mean} \quad (3.11)$$

347 Where  $h$  is the total heat transfer coefficient:

$$h = h_c + h_r \quad (3.12)$$

348 And  $h_r$  is the radiation heat transfer coefficient:

$$h_r \simeq \sigma \varepsilon 4 T_0^3 \quad (3.13)$$

349 Where  $\sigma$  is the Stefan-Boltzmann constant and  $\varepsilon$  is the average emissivity of the surfaces. Equations (3.11) and (3.12) assume that surface radiation, like surface convection, is governed by the 350 temperature difference between the surface and the interior. Let us interrogate the validity of this 351 assumption by imagining an idealized scenario. Consider a fictional body inside the space that follows 352 the interior temperature and exchanges radiant energy uniformly with all surrounding surfaces. This 353 fictional radiator does not heat the air directly, but it does heat the air indirectly at a later time 354 (because it heats or cools the mass, and later the mass heats or cools the air). Consider also that 355 when there is no radiator present, and the idealized space is empty, there is no net radiation exchange 356 when there is no radiator present, and the idealized space is empty, there is no net radiation exchange 357 between the enclosing surfaces since they are all the same temperature.

358 *3.3. Interior heat loads*

359 Can this fictional radiator be used as a proxy for internal heat loads? In a real room, there are 360 many kinds of heat sources and sinks, of different sizes, locations, and time signatures. Locally, they 361 heat or cool the interior air by convection. Remotely, they heat or cool other surfaces by radiation. 362 Real interior heat loads are not evenly distributed in space, nor are they harmoniously synchronized in 363 time. Moreover, recall that the direction of heating for the fictional radiator is  $\theta_i > \theta_s$  during the day, 364 switching to  $\theta_i < \theta_s$  during the night. Real interior heat loads may diminish or disappear at night, but 365 they do not spontaneously turn into sources of cooling.

366 Despite these inconsistencies and contradictions, a fictional radiator (which follows the interior 367 temperature) is still a relevant proxy for average heat loads. This radiator cannot represent realistic 368 heating distributions in time or space, because a harmonic model cannot account for the possible 369 knock-on effects of asymmetrical or asynchronous loads on the temperature evolution of the system. 370 Nevertheless, evaluating the effects of an average heat load is a useful starting point (c.f. §1 *strategic 371 models*)

372 To apply this proxy for internal heat loads, the analyst must first evaluate the heat flux from the  
 373 fictional radiator and decide if it needs increasing to meet any deficit in the expected average heat load.  
 374 Meeting the deficit can be done by multiplying  $h_r$  by some factor. Then the charging and discharging  
 375 cycles must be balanced over the day. For instance, by assuming that the ventilation openings ( $A^*$ )  
 376 are automatically increased at night, so the extra buoyancy ventilation matches the night cooling by  
 377 the fictional radiant body.

378 Figure 9 compares the cumulative surface heat transfer due to natural convection and radiation.  
 379 The yellow portions of the graph show natural convection, which is present even when the interior  
 380 space is empty. The red parts show emissions from a fictional radiator as a proxy for internal loads.  
 381 The graphs are arranged in a grid with two columns, one for each damping coefficient: the left-hand  
 382 column aligns with the peak venting temperature difference  $|\theta_e - \theta_i|_{peak}$ ; the right-hand column aligns  
 383 with attenuating temperature difference  $1 - 1/A_i$ . The top row of graphs shows a governing trend:  
 384 the larger the damping coefficient, the smaller the temperature difference between the surface and the  
 385 interior air. This downturn leads to slight reductions in the heat transfer coefficient ( $\text{W/m}^2\text{-K}$ , see  
 386 middle row), but considerable reductions in the surface heat flux ( $\text{W/m}^2$ , see bottom row).

387 Note that, in Figure 9, the radiant heat transfer coefficient is defined by equation Equation (3.13),  
 388 and the radiant heat flux is controlled by  $|\theta_s - \theta_i|_{mean}$  in Equation (3.11) (i.e. the radiant heat flux  
 389 has *not* been adjusted to equally represent internal loads for all values of either damping coefficient; in  
 390 this way, the relative changes and possible deficits are clear to see). Furthermore, note that the heat  
 391 flux is reported in terms of the unit surface area of the mass, not in terms of the unit floor area (which  
 392 is how internal loads are typically presented).

393 To compute the results shown in Figure 9, the environmental temperature was fixed at  $\Delta T =$   
 394 10 and  $T_0 = 20^\circ\text{C}$  (293.15 K). Optimal pairs of  $F/\lambda$  and  $\Omega$  are needed to calculate  $|\theta_s - \theta_i|_{mean}$  for  
 395 increments of  $|\theta_e - \theta_i|_{peak}$  and  $1 - 1/A_i$ . This was done by simultaneously solving Equations (3.2)  
 396 and (3.3) or Equations (3.5) and (3.6), assuming no surface temperature delay (i.e.  $\lambda = 1$ ). The  
 397 surface heat transfer was then computed following the procedure described in §3.2, assuming a large,  
 398 10 by 10 meter vertical surface for the convection calculations.

#### 399 4. Results and discussion

400 The previous section found optimal pairings for  $F/\lambda$  and  $\Omega$ , and explained how to approximately  
 401 account for internal loads by adjusting the heat transfer coefficient. This theory is now applied in some

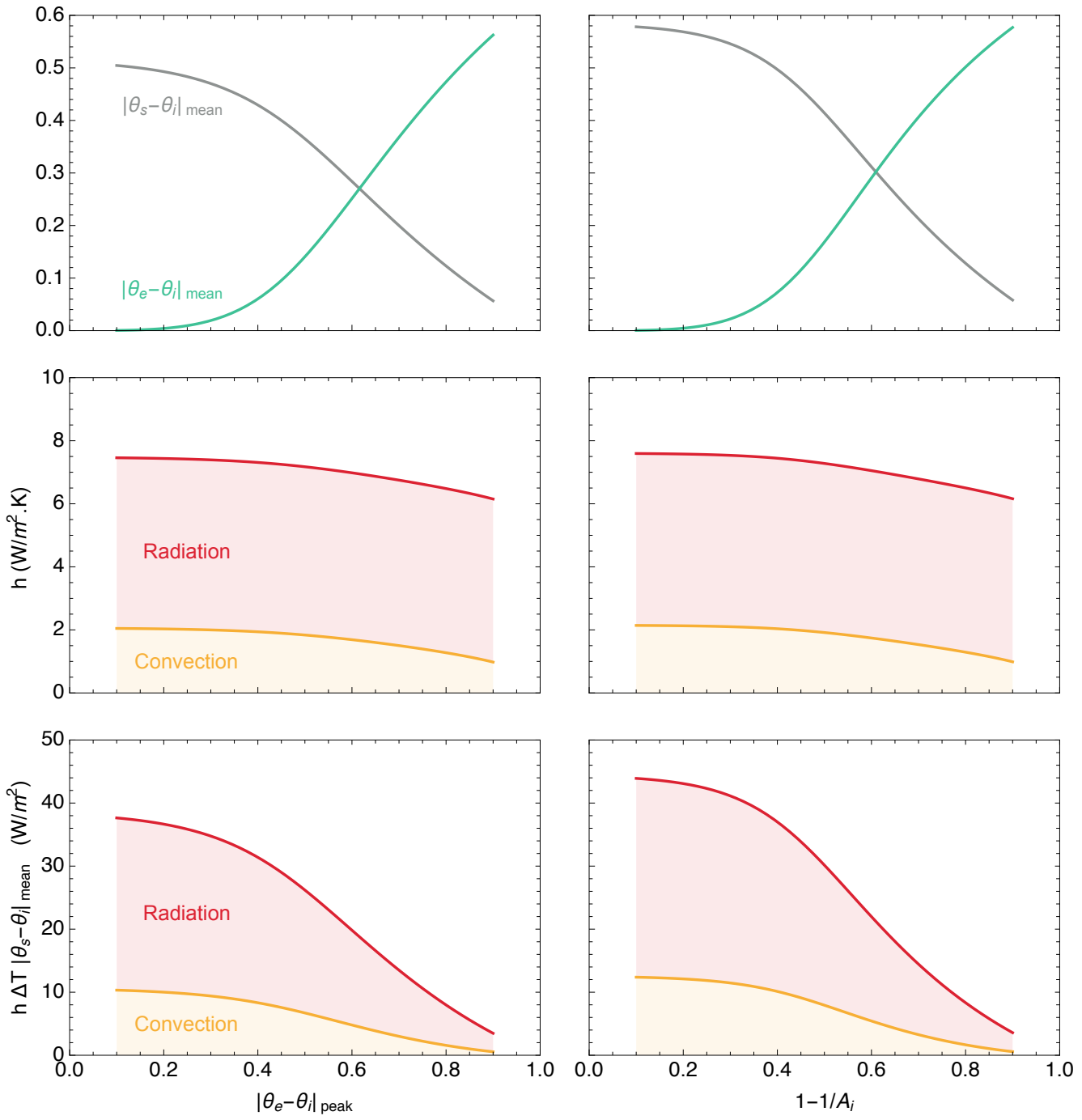
Figure 9: Variation of surface heat transfer with  $|\theta_e - \theta_i|_{\text{peak}}$  and  $1 - 1/A_i$

Table 1: Candidates for thermal mass: representative ranges for thermal properties and CO<sub>2</sub> footprints [97]

	k (W/m-K)	$\rho c$ (J/m <sup>3</sup> -K)	CO <sub>2</sub> footprint (kg/m <sup>3</sup> )
Steel	51.5 $\pm$ 2.5	(3.79 $\pm$ 0.20) $\times 10^6$	14135. $\pm$ 875.
Sandstone	5.70 $\pm$ 0.30	(2.16 $\pm$ 0.28) $\times 10^6$	87. $\pm$ 19.
Concrete	1.6 $\pm$ 0.8	(2.3 $\pm$ 0.4) $\times 10^6$	260. $\pm$ 53.
Glass	1.00 $\pm$ 0.30	(2.22 $\pm$ 0.15) $\times 10^6$	1850. $\pm$ 142.
Brick	0.59 $\pm$ 0.14	(1.49 $\pm$ 0.29) $\times 10^6$	402. $\pm$ 82.
Hardwood*	0.46 $\pm$ 0.05	(1.59 $\pm$ 0.18) $\times 10^6$	-400 $\pm$ 1300

\*Values for  $k$  assume conduction is parallel to the grain. Values for CO<sub>2</sub> footprint range from net storage to net release. Notice how, per unit volume, timber can sequester carbon or be worse than concrete, depending on how the forest is managed.

402 massing studies, which show the effect that optimal designs have on material quantities and physical  
 403 proportions.

#### 404 4.1. Materials comparison

405 Among practitioners, it is common knowledge that some materials are more effective as thermal  
 406 mass because of their thermal properties. (Namely: the thermal conductivity,  $k$  (W/m-K); the volu-  
 407 metric heat capacity,  $\rho c$  (J/m<sup>3</sup>-K); and the combination of these in a ratio called the thermal diffusivity,  
 408  $\alpha = k/\rho c$  (m<sup>2</sup>/s), which compares the internal rate of heat transfer to heat storage, indicating how  
 409 quickly heat spreads through a material.) However, when it comes to examining thermal mass ma-  
 410 terials in action, it is difficult to draw conclusions that meaningfully influence design—particularly in  
 411 the critical early stages—since it is hard to isolate the role that architectural properties play in the  
 412 co-evolution of system temperatures. What proportions should a thermally massive building have?  
 413 How should the thermal mass be distributed? Should the massing change with the choice of material?  
 414 Without comprehensive answers to these questions, analysts, when studying the effects of thermal  
 415 mass with dynamic models, have had little choice but to fix the dimensions of their control buildings  
 416 arbitrarily [98–100] —until now.

417 Table 1 gives ranges of thermal properties for some standard construction materials [97]. Figure 10  
 418 compares the efficiency of these materials as thermal mass when they are optimally tuned as part  
 419 of a thermal feedback cycle (c.f. Figure 3). That is, a building with internal mass that maximizes

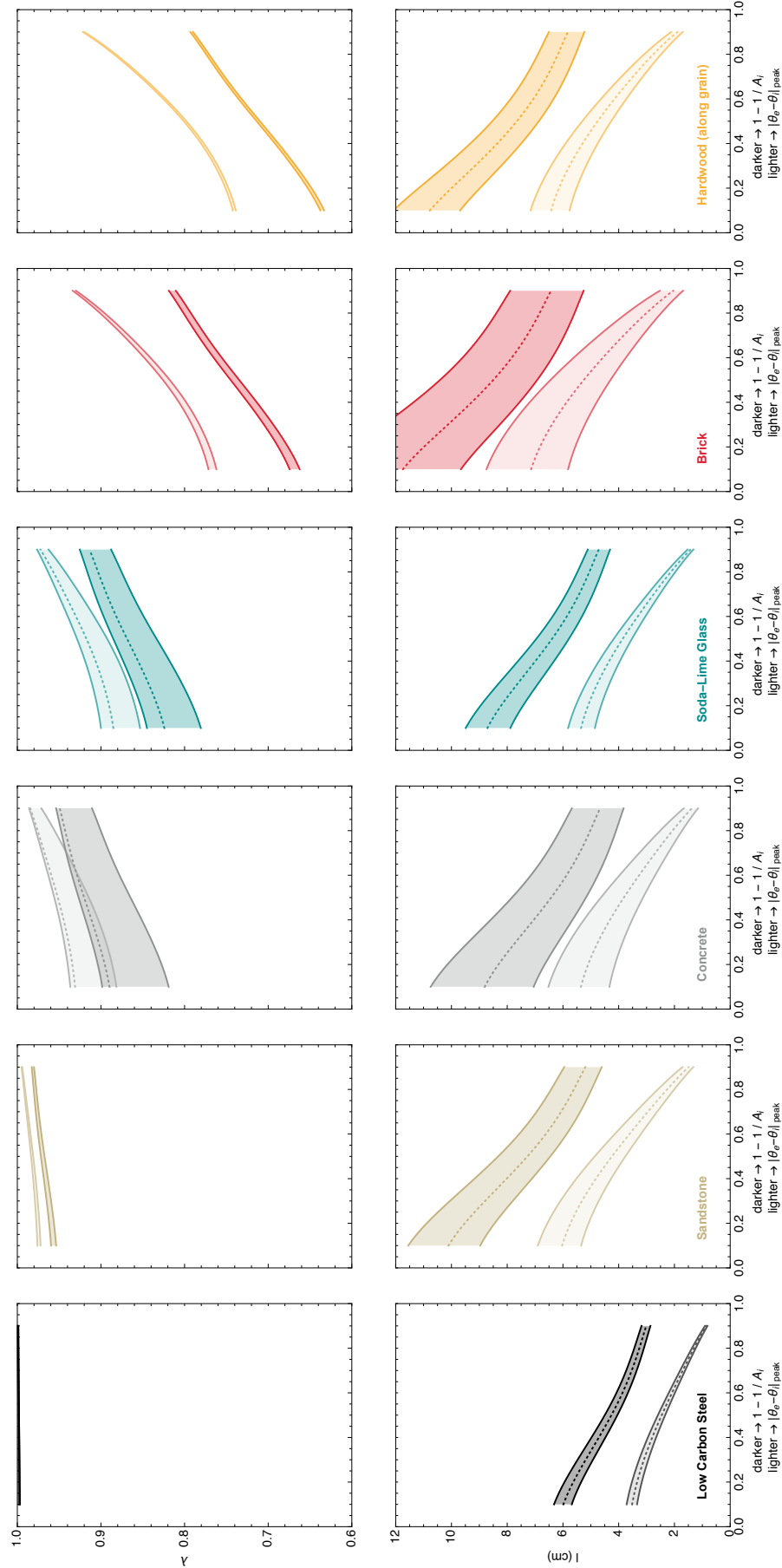


Figure 10: Optimal thicknesses (1) and resulting surface temperature lags ( $\lambda$ ) for various construction materials as a function of the damping coefficient,  $|\theta_e - \theta_i|_{peak}$  (light shading), or  $1 - 1/A_i$  (dark shading). The coloured bands depict the variation in thermal properties reported in Table 1.

420 buoyancy ventilation for a given damping coefficient ( $|\theta_e - \theta_i|_{peak}$ , light shading;  $1 - 1/A_i$ , dark shading).  
 421 Figure 10 shows the layer thicknesses ( $l$ , bottom row) and the divergence in surface temperatures ( $\lambda$ ,  
 422 top row) for different materials. The width of the coloured bands reflects the uncertainty associated  
 423 with the thermal properties (c.f. Table 1); the dotted lines assume average values for these properties.

424 Figure 10 is based on the same set of assumptions as Figure 9 (recall from §3.3 that the radiant heat  
 425 flux varies with  $|\theta_s - \theta_i|_{mean}$ ; it was *not* adjusted to model internal loads equally across all values of  
 426 the damping coefficient). Figure 10 can be reproduced with different inputs by following these three  
 427 steps:

- 428 • Choose a damping coefficient to optimize for ( $|\theta_e - \theta_i|_{peak}$  or  $1 - 1/A_i$ ) and find the associated  
 429 optimal values for  $\Omega$  (c.f. §3.1)
- 430 • Estimate  $h$  by: (a) Consulting Figure 8 and Figure 9. Or (b) estimate  $|\theta_s - \theta_i|_{mean}$  by setting  $\lambda$   
 431 = 1. Use this result to compute  $h$  (c.f. §3.2), incorporating an estimate for internal heat loads  
 432 as necessary (c.f. §3.3).
- 433 • Find the optimal thicknesses ( $l$ ) and resulting surface temperature delays ( $\lambda$ ) by simultaneously  
 434 solving Equations (2.22), (2.23) and (2.24). (A first approximation can be made by assuming  $\lambda$   
 435 = 1, so that  $l_r = 1$  and Equation (2.22) reduces to  $\Omega = \xi$ )

436 Figure 10 reveals some general trends, which reflect the balance of thermal relationships

- 437 • As either damping coefficient ( $|\theta_e - \theta_i|_{peak}$  or  $1 - 1/A_i$ ) increases, the optimal thickness reduces.  
 438 This is because the massing parameter,  $\Omega$ , and the surface heat flux,  $h \Delta T |\theta_s - \theta_i|_{mean}$ , reduce,  
 439 too.
- 440 • Optimizing for the damping coefficient  $|\theta_e - \theta_i|_{peak}$  results in relatively thinner masses, because  
 441 this damping coefficient is associated with smaller values of  $\Omega$ , and so requires less thermal  
 442 capacity.
- 443 • The uncertainty associated with thermal properties can lead to significant discrepancies in optimal  
 444 thickness—in the order of centimeters. In later stages of design, it is therefore important to obtain  
 445 more accurate values for thermal properties, ideally with direct measurements of actual samples.

446 Moreover, Figure 10 suggests several new findings regarding the efficiency of different construction  
 447 materials as thermal mass:

448     • Some natural stones and concretes are particularly efficient as an internal thermal mass when  
 449     optimally-tuned (which should come as no surprise since these materials have relatively high  
 450      $k$  and high  $\rho c$ ). *However, the ideal tuning adds new meaning to what constitutes an efficient*  
 451     *thermal mass.* The plots show that, when optimized, sandstone and concrete have non-divergent  
 452     surface temperatures ( $\lambda \rightarrow 1$ ). Recall that  $F = (F/\lambda) * \lambda$ . Therefore, compared to other optimized  
 453     masses, these masses are able to produce more ventilation for a given damping coefficient

454     • However, some concretes (those with lower  $k$  and  $\rho c$ ) do not perform as well. The function for  
 455      $\lambda$  (Equation (2.24)) is particularly sensitive in the range  $1 \lesssim \eta \lesssim 2$  (c.f. fig 8.b. in Holford and  
 456     Woods [12]). Optimally-tuned concrete is uniquely situated in this range, making it susceptible  
 457     to sudden (and unexpected) drops in efficiency. Consider that the thermal properties of concrete  
 458     (or any structural material for that matter) are rarely specified or measured in real projects.

459     • The graphs reveal many situations in which  $l \lesssim 5$  cm, suggesting that thin-shell structures of  
 460     minimum weight [101–107] may also be optimized for thermal mass and natural ventilation.

461     • Assuming the heat-flux is oriented parallel to the grain, optimally-tuned hardwood compares  
 462     well against brick and not too poorly against concrete. (The thermal conductivity of hardwood  
 463     perpendicular to the grain, and for softwoods in either grain orientation, are lower.) This sug-  
 464     gests it is possible to use some timbers as internal thermal mass—with reasonable effect. These  
 465     thermally resilient timber buildings could legitimately sequester carbon dioxide, so long as the  
 466     timbers are sourced from sustainable, managed forests, and the buildings last longer than the  
 467     growing cycles of these forests [97, 108–111].

468     • While not analyzed here, the thermal properties of earthen materials [112] and high-density  
 469     bamboo composites [113] suggest that these materials are promising candidates, too.

470     *4.2. Fixed volume of material*

471     The remainder of this section examines the consequences of the ideal tuning in terms of building  
 472     dimensions, material quantities, and ventilation rates.

473     Figure 11 shows how to distribute *a fixed amount* of concrete thermal mass inside an insulated  
 474     cuboid of height  $H = 10$ m. The floor area is variable, but constrained to the shape of a square ( $W^2$ ),  
 475     thereby defining the geometry of the ceiling and four walls where the mass is distributed. Since  $V = S$   
 476      $l$ , optimally distributing a fixed volume of material ( $V$ ) means finding the balance of surface area ( $S$ )  
 477     and thickness ( $l$ ) that:

478     • Meets a given damping coefficient (i.e. a design value for  $|\theta_e - \theta_i|_{peak}$  or  $1 - 1/A_i$  ), while;

479     • Maximizing the rate of buoyancy ventilation (Q).

480     The calculation flow for producing Figure 11 follows these steps:

481     • Find the ideal tuning for  $\Omega$  and  $F/\lambda$  (c.f. §3.1)

482     • Estimate  $h$  and find  $l$  and  $\lambda$  (c.f. §4.1)

483     • Now  $S = V/l$  and  $Q = \frac{F S h}{\rho_i c_i}$  (c.f. Equation (2.25))

484     • Furthermore, though not shown in Figure 11,  $A* = \frac{Q}{\sqrt{\beta g H \Delta T |\theta_e - \theta_i|_{mean}}}$  (c.f. Equation (2.27))

485     Here are some things to bear in mind when reading Figure 11:

486     • The concrete mix assumes mean values for thermal properties shown in Table 1. The environmental temperature and the rates of surface heat transfer are the same as those described in §3.3 and shown in Figure 9.

489     • For the purposes of demonstration, the volume of concrete is arbitrarily fixed at  $V = \{8, 27, 64\}$   $m^3$ .

492     • For reference, when the ratio of width to height is  $W/H = \{1, 2, 3, 4\}$ , the surface area of the thermal mass is  $S = \{500, 1200, 2100, 3200\} m^2$

495     • For reference, a sufficient amount of ventilation for one person is typically 10 liters per second. That is,  $Q = 0.01 m^3/s$ . Therefore, when the ventilation rate is  $Q = \{0.1, 1, 10\} m^3/s$ , there is enough fresh air for approximately  $\{10, 100, 1000\}$  people.

496     Some general observations can be made:

497     • Optimizing for the attenuating temperature difference requires thicker masses, resulting in smaller buildings (compared to the peak venting temperature difference, when the material volume is fixed).

500     • The relative power distribution, shown in the bottom row of graphs, does not change with the volume constraint (since the balance of thermal exchanges is the same for each optimal case).

502     While it is unconventional to fix the amount of material before design commences, this strategy may 503     be useful in the coming decade as carbon caps become better defined and more stringent.

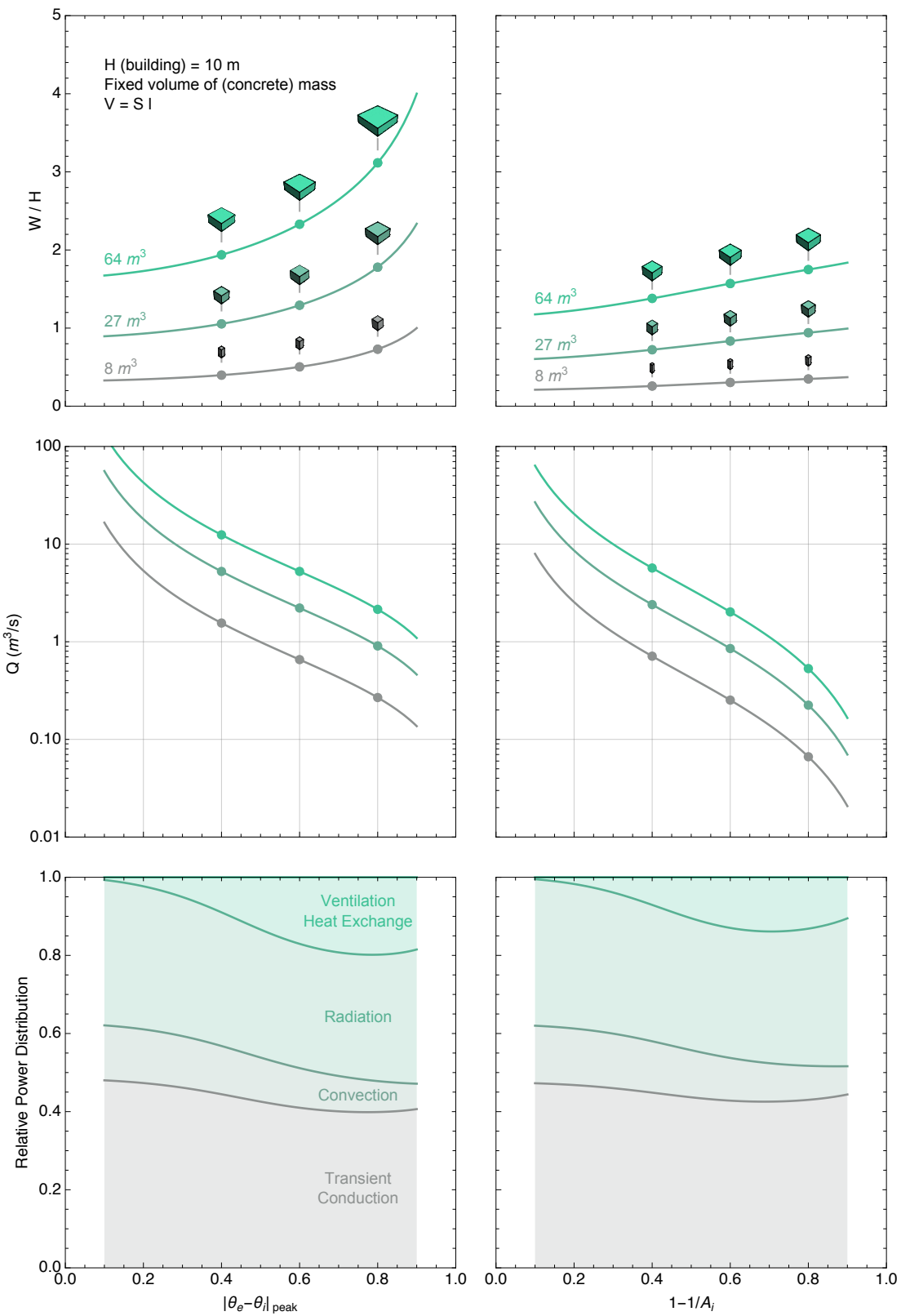


Figure 11: The optimal distribution of a fixed amount of concrete thermal mass ( $V = S l$ ) that maximizes buoyancy ventilation ( $Q$ ) for a given damping coefficient ( $|\theta_e - \theta_i|_{peak}$  or  $1 - 1/A_i$ )

504 4.3. *Fixed rate of ventilation*505 Having shown how to use the ideal tuning to compare massings made from the same volume of  
506 material, this subsection compares ideally-tuned massings that produce the same ventilation.507 Figure 12 shows how to distribute *the ideal amount* of concrete thermal mass inside an insulated  
508 cuboid of height  $H = 10\text{m}$ . The rate of buoyancy ventilation is fixed at  $Q = \{1, 10\} \text{ m}^3/\text{s}$  to provide  
509 enough fresh air for approximately  $\{10, 100\}$  people. Since  $V = S l$ , finding the ideal volume of concrete  
510 ( $V$ ) means finding the combination of surface area ( $S$ ) and thickness ( $l$ ) that:511 • Meets a given damping coefficient (i.e. a design value for  $|\theta_e - \theta_i|_{peak}$  or  $1 - 1/A_i$  ), while;  
512 • Meeting the target rate of buoyancy ventilation ( $Q$ ).

513 The calculation flow for producing Figure 12 follows these steps:

514 • Find the ideal tuning for  $\Omega$  and  $F/\lambda$   
515 • Find  $l$  and  $\lambda$   
516 • Now  $S = \frac{Q \rho_i c_i}{F h}$  and  $V = S l$ 

517 Here are some things to bear in mind when reading Figure 12:

518 • The assumptions (thermal properties, environmental temperature, surface heat transfer) are the  
519 same as in Figure 11.  
520 • Unlike Figure 11, the vertical axis for  $W/H$  is logarithmic  
521 • The images of the cuboids are scaled to the largest cuboid in the graph (hence they appear  
522 smaller than the cuboids in Figure 11).523 Compared to figure 11, the ideal proportions ( $W/H$ ) in Figure 12 vary considerably, since there is no  
524 constraint on the material volume. One range worth taking a closer look at is the range of damping  
525 coefficient  $0.6 \lesssim 1 - 1/A_i \lesssim 0.8$  when  $Q = 1 \text{ m}^3/\text{s}$ . These massings perform well without needing a  
526 very large surface ( $W/H < 10$ ) or a very large amount of concrete ( $V < 100\text{m}^3$ )527 Figure 13 interrogates this range in more detail, using different geometries and comparing the  
528 efficacy of concrete to timber (hardwood, parallel to the grain, c.f. Table 1) as internal thermal mass.  
529 The buildings start as a hemisphere or a cube ( $H = 10 \text{ m}$ ). Their shapes then 'morph' according to

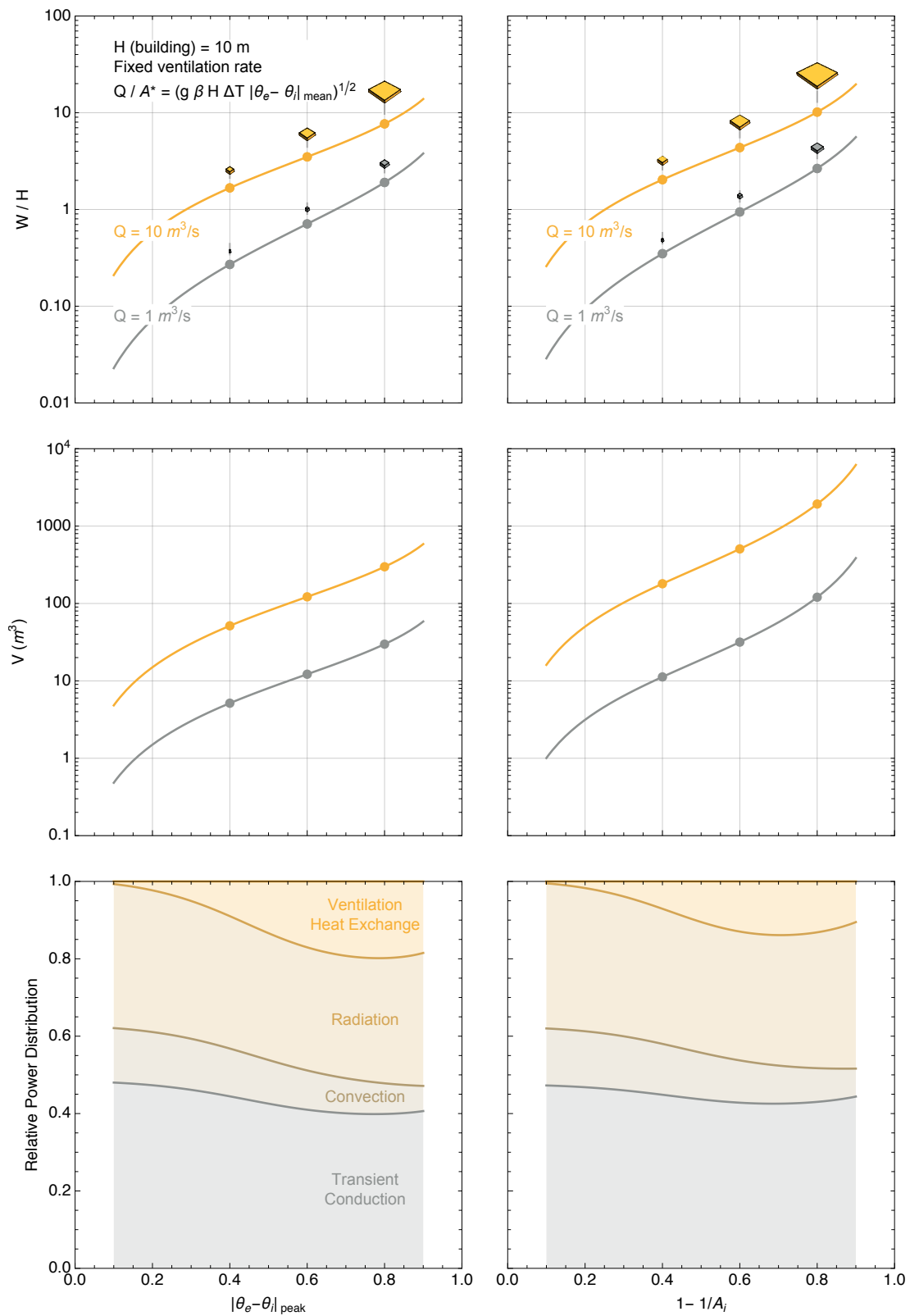


Figure 12: Optimal quantities ( $V = Sl$ ) and distributions ( $W/H$ ) of thermal mass for a fixed ventilation rate ( $Q$ ) to meet a target interior floating temperature ( $e-i$  peak or  $1-1/A_i$ ).

530 mathematically defined rules, which allow the surface area of the building to increase without taking up  
 531 much extra land. As the surface area increases, so does the damping coefficient—though the ventilation  
 532 is always the same. Bluer colours, therefore, indicate cooler buildings.

533 Figure 13 shows three columns of "morph sequences". These morphologies are defined as follows:

534 • **Blobs.** These surfaces are defined by the Legendre polynomial  $P_n(x)$  [114], plotted in spherical  
 535 coordinates, such that: the radius is  $r = 1 + c P_n(\cos(\phi)) \cos(\vartheta)$ ; the zenith (latitude) angles  
 536 are  $0 \leq \phi \leq \pi$ ; and the azimuth (longitude) angles are  $0 \leq \vartheta \leq \pi$ . The coefficient  $c$  (here set to  
 537  $c = 1/4$ ) determines the "smoothness" of the polynomial and hence the smoothness of the blob.  
 538 The integer  $n$  increases the number of operations in the polynomial and hence the number of  
 539 "wings" the blob has.

540 • **Castles.** The remaining two columns are populated by surfaces defined by fractals: a Sierpiński  
 541 space-filling curve [115], and a Cesàro fractal [116] —which in this case is made by drawing a  
 542 Koch curve [117] with angles of  $85^\circ$ .

543 The morphologies are stylistically distinct, but follow the same thermal proportions. While the ideal  
 544 tuning for thermal mass governs bulk dimensions, material quantities, temperature attenuation, and  
 545 buoyancy ventilation, it does not overly determine the choice of form or the spatial layout. Nor  
 546 does it overly determine the choice of thermal mass material. As the performance data in Figure 13  
 547 show, concrete outperforms hardwood thermally—but surprisingly not by very much. (The hardwood  
 548 versions have slightly lower values for  $\lambda$ , hence  $1 - 1/A_i$  is slightly reduced. The ventilation rate is  
 549 maintained at  $Q = 1 \text{ m}^3/\text{s}$  by slightly increasing  $A_*$ )

550 Notice how the wings, courtyard niches, and open plans in Figure 13 would have very different  
 551 consequences for the inter-subjective experience of occupants. Working with the ideal massing ratios  
 552 ( $F/\lambda, \Omega$ ) can profoundly but playfully shape the development of an architectural concept from *part to*  
 553 *whole*—from the type and thickness of the massing material to the spatial organization of the building.

#### 554 4.4. Limitations

555 The method is meant to support concept generation and guide engineering studies towards conver-  
 556 gence. It is tailored for strategic comparisons at the early stage of design, not absolute forecasts at  
 557 the later stages of design (c.f. §1). The value for the heat transfer coefficient must be chosen carefully  
 558 to fairly represent surface heat transfer (c.f. §3.2) and serve as a suitable proxy for average internal

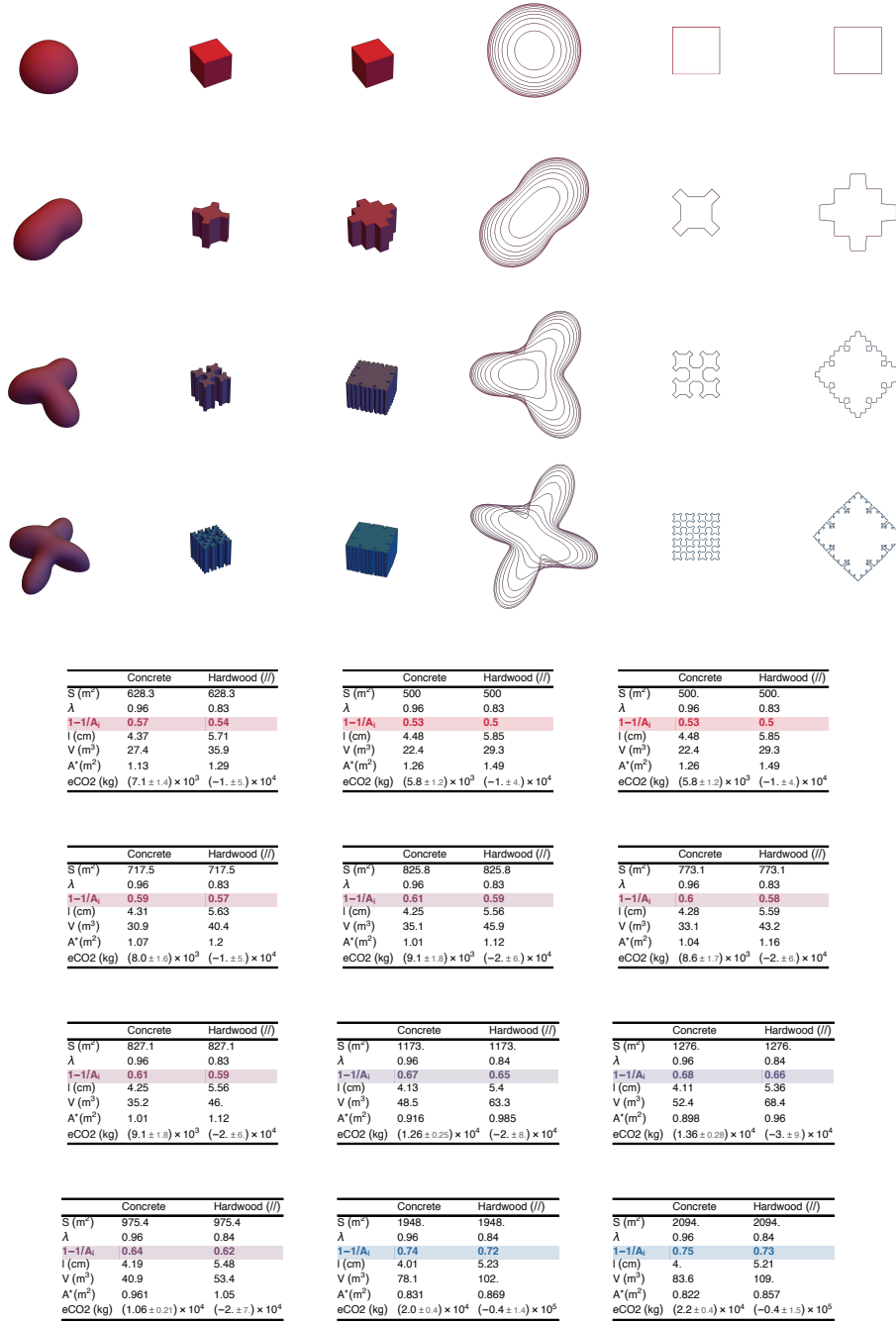


Figure 13: Blobs and castles. These optimized massings have different architectural styles, but all have height  $H = 10$  m and ventilation enough for 100 people ( $Q = 1 \text{ m}^3/\text{s}$ ). As the surface area increases, the floating interior temperature ( $1-1/A_i$ ) cools, and the optimal thickness of thermal mass reduces. Concrete outperforms hardwood thermally, but surprisingly not by very much.

559 loads (c.f. §3.3). A representative range of thermal property values should be used for each candidate  
560 material, to reflect the uncertain variation of these properties in the real world (c.f. §4.1). Once a  
561 configuration for the building is chosen, Equation (2.16) or Equation (2.17) should be solved to more  
562 accurately establish the free-running temperature and ventilation rate. Then further analysis is needed  
563 to test the detailed response in a range of scenarios (e.g. anharmonic loads from inside and outside)  
564 and to finalize the design (e.g. external insulation, windows, supplementary heating or cooling). One  
565 particularly important thing to analyze is how the balance of buoyancy forces, heat loads, and heat  
566 storage effects may play out over short and long time scales (§2.1).

## 567 5. Conclusion

568 §1 outlined the need for a new approach to building design in the early stages, which allows teams to  
569 evaluate the environmental impacts of primary material choices while showing them how to integrate  
570 as many functions into these primary materials as possible, so there is less need for other materi-  
571 als, products, and technologies, shrinking the ecological footprint. Shaping one material to integrate  
572 structure, thermal mass, and buoyancy ventilation, is a prominent place to start.

573 §2 showed that, while there has been lots of progress on efficient methods for simulating the effects  
574 of thermal mass in arbitrary configurations, none of this new knowledge has been distilled for architects  
575 and planners wanting to know how to proportion thermally massive buildings properly, particularly in  
576 light of challenges posed by climate change. The work by Holford and Woods [12] was identified as a  
577 promising basis for this much-needed design guidance.

578 §3 found how to optimally synchronize the coupling of internal thermal mass and buoyancy venti-  
579 lation. The performance of the building is defined by relationship between two parameters:  $F/\lambda$  (the  
580 ratio of ventilation heat transfer to surface heat transfer) and  $\Omega$  (the ratio of thermal storage to surface  
581 heat transfer). When converted into optimal values, these parameters represent ideal ratios for tuning  
582 the form and mass of the building. Design teams can use these ratios to meet chosen targets for the  
583 interior temperature and ventilation rate in free-running mode and meaningfully compare the material  
584 footprint of design proposals.

585 §4 demonstrated how to take these ideal ratios ( $F/\lambda$ ,  $\Omega$ ) and materialize them into possible design  
586 options. One of the studies suggested that thin-shell structures of minimum weight, and even timber  
587 buildings, may be optimally tuned to produce ample ventilation and temperature attenuation (c.f.  
588 §4.1). Another study showed how working with these ideal ratios ( $F/\lambda$ ,  $\Omega$ ) could profoundly but

589 playfully shape the development of an architectural concept from part to whole, including the spatial  
590 organization of the building, which determines the possible social interactions (c.f. §4.3).

## 591 References

592 [1] H. King, S. Ocko, L. Mahadevan, Termite mounds harness diurnal temperature oscillations for ventilation, *Proceedings of the National Academy of Sciences* 112 (37) (2015) 11589–11593. doi:10.1073/pnas.1423242112.

593 [2] S. A. Ocko, H. King, D. Andreen, P. Bardunias, J. S. Turner, R. Soar, L. Mahadevan, Solar-powered ventilation  
594 of African termite mounds, *Journal of Experimental Biology* 220 (18) (2017) 3260–3269. doi:10.1242/jeb.160895.

595 [3] S. Craig, Termite mound climate control (Dec 2017).  
596 URL <https://massivesci.com/articles/termite-mound-arcology-climate-control/>

597 [4] S. A. Ocko, A. Heyde, L. Mahadevan, Morphogenesis of termite mounds, *Proceedings of the National Academy of  
598 Sciences* 116 (9) (2019) 3379–3384. doi:10.1073/pnas.1818759116.

599 [5] M. Vellinga, P. Oliver, A. Bridge, *Atlas of Vernacular Architecture of the World*, Routledge, 2007.

600 [6] W. Addis, *Building: 3000 years of design engineering and construction*, Phaidon, 2007.

601 [7] N. Cardinale, G. Rospi, P. Stefanizzi, Energy and microclimatic performance of Mediterranean vernacular build-  
602 ings: The Sassi district of Matera and the Trulli district of Alberobello, *Building and Environment* 59 (2013)  
603 590–598. doi:10.1016/j.buildenv.2012.10.006.

604 [8] *Passive Solar Buildings*, MIT Press, 1992.

605 [9] J. Clarke, *Energy Simulation in Building Design*, Routledge, 2007.

606 [10] C. Underwood, F. Yik, *Modelling Methods for Energy in Buildings*, John Wiley & Sons, 2008.

607 [11] J. D. Balcomb, Passive solar research and practice, *Energy and Buildings* 7 (4) (1984) 281–295. doi:10.1016/0378-  
608 7788(84)90074-4.

609 [12] J. M. Holford, A. W. Woods, On the thermal buffering of naturally ventilated buildings through internal thermal  
610 mass, *Journal of Fluid Mechanics* 580 (2007) 3–29. doi:10.1017/S0022112007005320.

611 [13] B. Lishman, A. W. Woods, The effect of gradual changes in wind speed or heat load on natural ventilation in a  
612 thermally massive building, *Building and Environment* 44 (4) (2009) 762–772. doi:10.1016/j.buildenv.2008.06.026.

613 [14] G. Reynders, T. Nuyttten, D. Saelens, Potential of structural thermal mass for demand-side management in  
614 dwellings, *Building and Environment* 64 (2013) 187–199. doi:10.1016/j.buildenv.2013.03.010.

615 [15] S. I. Seneviratne, M. G. Donat, A. J. Pitman, R. Knutti, R. L. Wilby, Allowable CO<sub>2</sub> emissions based on regional  
616 and impact-related climate targets, *Nature* 529 (7587) (2016) 477–483. doi:10.1038/nature16542.

617 [16] C. A. Kennedy, I. Stewart, A. Facchini, I. Cersosimo, R. Mele, B. Chen, M. Uda, A. Kansal, A. Chiu, K. gon Kim,  
618 C. Dubeux, E. L. L. Rovere, B. Cunha, S. Pincetl, J. Keirstead, S. Barles, S. Pusaka, J. Gunawan, M. Adegbile,  
619 M. Nazariha, S. Hoque, P. J. Marcotullio, F. G. Otharán, T. Genena, N. Ibrahim, R. Farooqui, G. Cervantes,  
620 A. D. Sahin, Energy and material flows of megacities, *Proceedings of the National Academy of Sciences* 112 (19)  
621 (2015) 5985–5990. doi:10.1073/pnas.1504315112.

622 [17] J. M. Allwood, M. F. Ashby, T. G. Gutowski, E. Worrell, Material efficiency: providing material services with less

624 material production, *Philosophical Transactions of the Royal Society of London A: Mathematical, Physical and*  
625 *Engineering Sciences* 371 (1986) (2013) 20120496. doi:10.1098/rsta.2012.0496.

626 [18] F. Pomponi, C. D. Wolf, A. Moncaster, *Embodied Carbon in Buildings: Measurement, Management, and Mitiga-*  
627 *tion*, Springer, 2018.

628 [19] B. King, *The New Carbon Architecture: Building to Cool the Climate*, New Society Publishers, 2017.

629 [20] C. D. Wolf, F. Pomponi, A. Moncaster, Measuring embodied carbon dioxide equivalent of buildings: A review and  
630 critique of current industry practice, *Energy and Buildings* 140 (2017) 68–80. doi:10.1016/j.enbuild.2017.01.075.

631 [21] F. Pomponi, A. Moncaster, C. D. Wolf, Furthering embodied carbon assessment in practice: Re-  
632 sults of an industry-academia collaborative research project, *Energy and Buildings* 167 (2018) 177–186.  
633 doi:10.1016/j.enbuild.2018.02.052.

634 [22] F. Pomponi, A. Moncaster, Briefing: BS 8001 and the built environment: a review and critique, *Proceedings of*  
635 *the Institution of Civil Engineers - Engineering Sustainability* 172 (3) (2018) 111–114. doi:10.1680/jensu.17.00067.

636 [23] A. M. Moncaster, F. Pomponi, K. E. Symons, P. M. Guthrie, Why method matters: Temporal, spatial and  
637 physical variations in LCA and their impact on choice of structural system, *Energy and Buildings* 173 (2018)  
638 389–398. doi:10.1016/j.enbuild.2018.05.039.

639 [24] A. Dubois, L.-E. Gadde, The construction industry as a loosely coupled system: implications for productivity and  
640 innovation, *Construction Management and Economics* 20 (7) (2002) 621–631. doi:10.1080/01446190210163543.

641 [25] M. F. Ashby, J. Fernandez, A. Gray, *Unit 9. Architecture & Built Environment: Materials for Construction*.  
642 Granta CES EduPack 2007 (2007).

643 [26] B. D'Amico, F. Pomponi, A compactness measure of sustainable building forms, *Royal Society Open Science* 6 (6)  
644 (2019) 181265. doi:10.1098/rsos.181265.

645 [27] S. C. Sherwood, M. Huber, An adaptability limit to climate change due to heat stress, *Proceedings of the National*  
646 *Academy of Sciences* 107 (21) (2010) 9552–9555. doi:10.1073/pnas.0913352107.

647 [28] J. S. Pal, E. A. B. Eltahir, Future temperature in southwest Asia projected to exceed a threshold for human  
648 adaptability, *Nature Climate Change* 6 (2) (2016) 197–200. doi:10.1038/nclimate2833.

649 [29] G. P. Henze, J. Pfafferott, S. Herkel, C. Felsmann, Impact of adaptive comfort criteria and heat waves on optimal  
650 building thermal mass control, *Energy and Buildings* 39 (2) (2007) 221–235. doi:10.1016/j.enbuild.2006.06.006.

651 [30] S. Kumar, P. Tewari, S. Mathur, J. Mathur, Development of mathematical correlations for indoor temperature  
652 from field observations of the performance of high thermal mass buildings in India, *Building and Environment* 122  
653 (2017) 324–342. doi:10.1016/j.buildenv.2017.06.030.

654 [31] L.-S. Wang, P. Ma, E. Hu, D. Giza-Sisson, G. Mueller, N. Guo, A study of building envelope and thermal  
655 mass requirements for achieving thermal autonomy in an office building, *Energy and Buildings* 78 (2014) 79–88.  
656 doi:10.1016/j.enbuild.2014.04.015.

657 [32] S. Manu, Y. Shukla, R. Rawal, L. E. Thomas, R. de Dear, Field studies of thermal comfort across multiple climate  
658 zones for the subcontinent: India Model for Adaptive Comfort (IMAC), *Building and Environment* 98 (2016)  
659 55–70. doi:https://doi.org/10.1016/j.buildenv.2015.12.019.

660 [33] L. A. López-Pérez, J. J. Flores-Prieto, C. Ríos-Rojas, Adaptive thermal comfort model for ed-  
661 ucational buildings in a hot-humid climate, *Building and Environment* 150 (2019) 181–194.

662 doi:<https://doi.org/10.1016/j.buildenv.2018.12.011>.

663 [34] M. Vellei, M. Herrera, D. Fosas, S. Natarajan, The influence of relative humidity on adaptive thermal comfort, Building and Environment 124 (2017) 171–185. doi:<https://doi.org/10.1016/j.buildenv.2017.08.005>.

664 [35] E. Barbadilla-Martín, J. M. S. Lissén, J. G. Martín, P. Aparicio-Ruiz, L. Brotas, Field study on adaptive thermal comfort in mixed mode office buildings in southwestern area of Spain, Building and Environment 123 (2017) 163–175. doi:<https://doi.org/10.1016/j.buildenv.2017.06.042>.

665 [36] S. Carlucci, L. Bai, R. de Dear, L. Yang, Review of adaptive thermal comfort models in built environmental regulatory documents, Building and Environment 137 (2018) 73–89. doi:<https://doi.org/10.1016/j.buildenv.2018.03.053>.

666 [37] A. García, F. Olivieri, E. Larrumbide, P. Ávila, Thermal comfort assessment in naturally ventilated offices located in a cold tropical climate, Bogotá, Building and Environment 158 (2019) 237–247. doi:<https://doi.org/10.1016/j.buildenv.2019.05.013>.

667 [38] R. de Dear, J. Kim, T. Parkinson, Residential adaptive comfort in a humid subtropical climate—Sydney Australia, Energy and Buildings 158 (2018) 1296–1305. doi:<https://doi.org/10.1016/j.enbuild.2017.11.028>.

668 [39] Y. Song, Y. Sun, S. Luo, Z. Tian, J. Hou, J. Kim, T. Parkinson, R. de Dear, Residential adaptive comfort in a humid continental climate – Tianjin China, Energy and Buildings 170 (2018) 115–121. doi:<https://doi.org/10.1016/j.enbuild.2018.03.083>.

669 [40] D. Sánchez-García, C. Rubio-Bellido, J. J. M. del Río, A. Pérez-Fargallo, Towards the quantification of energy demand and consumption through the adaptive comfort approach in mixed mode office buildings considering climate change, Energy and Buildings 187 (2019) 173–185. doi:<https://doi.org/10.1016/j.enbuild.2019.02.002>.

670 [41] J. Kim, R. de Dear, T. Parkinson, C. Candido, Understanding patterns of adaptive comfort behaviour in the Sydney mixed-mode residential context, Energy and Buildings 141 (2017) 274–283. doi:<https://doi.org/10.1016/j.enbuild.2017.02.061>.

671 [42] E. Barbadilla-Martín, J. G. Martín, J. M. S. Lissén, J. S. Ramos, S. Álvarez Domínguez, Assessment of thermal comfort and energy savings in a field study on adaptive comfort with application for mixed mode offices, Energy and Buildings 167 (2018) 281–289. doi:<https://doi.org/10.1016/j.enbuild.2018.02.033>.

672 [43] A. Pérez-Fargallo, J. A. Pulido-Arcas, C. Rubio-Bellido, M. Trebilcock, B. Piderit, S. Attia, Development of a new adaptive comfort model for low income housing in the central-south of chile, Energy and Buildings 178 (2018) 94–106. doi:<https://doi.org/10.1016/j.enbuild.2018.08.030>.

673 [44] E.-S. Im, J. S. Pal, E. A. B. Eltahir, Deadly heat waves projected in the densely populated agricultural regions of South Asia, *Science Advances* 3 (8) (2017) e1603322. doi:10.1126/sciadv.1603322.

674 [45] S. Kang, E. A. B. Eltahir, North China Plain threatened by deadly heatwaves due to climate change and irrigation, *Nature Communications* 9 (1) (2018) 2894. doi:10.1038/s41467-018-05252-y.

675 [46] Q. Schiermeier, Climate change made Europe's mega-heatwave five times more likely, *Nature* (July 2019).

676 [47] C. Inard, J. Pfafferott, C. Ghiaus, Free-running temperature and potential for free cooling by ventilation: A case study, Energy and Buildings 43 (10) (2011) 2705–2711. doi:<https://doi.org/10.1016/j.enbuild.2011.06.017>.

677 [48] C. Ghiaus, Equivalence between the load curve and the free-running temperature in energy estimating methods, Energy and Buildings 38 (5) (2006) 429–435. doi:<https://doi.org/10.1016/j.enbuild.2005.08.003>.

678 [49] M. J. Holmes, J. N. Hacker, Climate change, thermal comfort and energy: Meeting the design challenges of the

700 21st century, *Energy and Buildings* 39 (7) (2007) 802–814. doi:10.1016/j.enbuild.2007.02.009.

701 [50] M. H. Kurth, J. M. Keenan, M. Sasani, I. Linkov, Defining resilience for the US building industry, *Building*  
702 *Research & Information* 47 (4) (2019) 480–492. doi:10.1080/09613218.2018.1452489.

703 [51] A. Baniassadi, J. Heusinger, D. J. Sailor, Energy efficiency vs resiliency to extreme heat and power  
704 outages: The role of evolving building energy codes, *Building and Environment* 139 (2018) 86–94.  
705 doi:<https://doi.org/10.1016/j.buildenv.2018.05.024>.

706 [52] D. Coley, M. Herrera, D. Fosas, C. Liu, M. Vellei, Probabilistic adaptive thermal comfort for resilient design,  
707 *Building and Environment* 123 (2017) 109–118. doi:<https://doi.org/10.1016/j.buildenv.2017.06.050>.

708 [53] K. J. Lomas, R. Giridharan, Thermal comfort standards, measured internal temperatures and thermal resilience  
709 to climate change of free-running buildings: A case-study of hospital wards, *Building and Environment* 55 (2012)  
710 57–72. doi:10.1016/j.buildenv.2011.12.006.

711 [54] L. Yang, Y. Li, Cooling load reduction by using thermal mass and night ventilation, *Energy and Buildings* 40 (11)  
712 (2008) 2052–2058. doi:10.1016/j.enbuild.2008.05.014.

713 [55] E. Krüger, E. G. Cruz, B. Givoni, Effectiveness of indirect evaporative cooling and thermal mass in a hot arid  
714 climate, *Building and Environment* 45 (6) (2010) 1422–1433. doi:10.1016/j.buildenv.2009.12.005.

715 [56] S. Verbeke, A. Audenaert, Thermal inertia in buildings: A review of impacts across climate and building use,  
716 *Renewable and Sustainable Energy Reviews* 82 (2018) 2300–2318. doi:10.1016/j.rser.2017.08.083.

717 [57] D. G. L. Samuel, S. M. S. Nagendra, M. P. Maiya, Passive alternatives to mechanical air conditioning of building:  
718 A review, *Building and Environment* 66 (2013) 54–64. doi:10.1016/j.buildenv.2013.04.016.

719 [58] P. Ma, L. S. Wang, Effective heat capacity of interior planar thermal mass (iPTM) subject to periodic heating  
720 and cooling, *Energy and Buildings* 47 (2012) 44–52. doi:10.1016/j.enbuild.2011.11.020.

721 [59] P. F. Linden, G. F. Lane-Serff, D. A. Smeed, Emptying filling boxes: The fluid mechanics of natural ventilation,  
722 *Journal of Fluid Mechanics* 212 (1990) 309–335. doi:10.1017/S0022112090001987.

723 [60] P. F. Linden, The Fluid Mechanics of Natural Ventilation, *Annual Review of Fluid Mechanics* 31 (1) (1999)  
724 201–238. doi:10.1146/annurev.fluid.31.1.201.

725 [61] A. Acred, Natural ventilation in multi-storey buildings: a preliminary design approach (September 2014).

726 [62] T. Chenvidyakarn, *Buoyancy effects on natural ventilation*, Cambridge University Press, Cambridge ; New York,  
727 2013.

728 [63] A. W. Woods, S. Fitzgerald, S. Livermore, A comparison of winter pre-heating requirements for nat-  
729 ural displacement and natural mixing ventilation, *Energy and Buildings* 41 (12) (2009) 1306–1312.  
730 doi:10.1016/j.enbuild.2009.07.030.

731 [64] A. S. Kuesters, A. W. Woods, A comparison of winter heating demand using a distributed and a point source of  
732 heating with mixing ventilation, *Energy and Buildings* 55 (2012) 332–340. doi:10.1016/j.enbuild.2012.07.045.

733 [65] A. Acred, G. R. Hunt, A simplified mathematical approach for modelling stack ventilation in multi-compartment  
734 buildings, *Building and Environment* 71 (2014) 121–130. doi:10.1016/j.buildenv.2013.09.004.

735 [66] A. Acred, G. R. Hunt, Stack ventilation in multi-storey atrium buildings: A dimensionless design approach,  
736 *Building and Environment* 72 (2014) 44–52. doi:10.1016/j.buildenv.2013.10.007.

737 [67] S. A. Gage, G. R. Hunt, P. F. Linden, Top down ventilation and cooling, *Journal of Architectural and Planning*

738 Research 18 (4) (2001) 286–301.

739 [68] T. Chenvidyakarn, A. Woods, Stratification and oscillations produced by pre-cooling during transient natural  
740 ventilation, *Building and Environment* 42 (1) (2007) 99–112. doi:10.1016/j.buildenv.2005.08.007.

741 [69] T. Chenvidyakarn, A. Woods, Top-down precooled natural ventilation, *Building Services Engineering Research*  
742 and *Technology* 26 (3) (2005) 181–193. doi:10.1191/0143624405bt129oa.

743 [70] S. R. Livermore, A. W. Woods, On the effect of distributed cooling in natural ventilation, *Journal of Fluid*  
744 *Mechanics* 600 (2008) 1–17. doi:10.1017/S0022112007009809.

745 [71] J. Yam, Y. Li, Z. Zheng, Nonlinear coupling between thermal mass and natural ventilation in buildings, *International*  
746 *Journal of Heat and Mass Transfer* 46 (7) (2003) 1251–1264. doi:10.1016/S0017-9310(02)00379-4.

747 [72] J. Zhou, G. Zhang, Y. Lin, Y. Li, Coupling of thermal mass and natural ventilation in buildings, *Energy and*  
748 *Buildings* 40 (6) (2008) 979–986. doi:10.1016/j.enbuild.2007.08.001.

749 [73] J. Zhou, G. Zhang, Y. Lin, H. Wang, A new virtual sphere method for estimating the role of thermal mass in  
750 natural ventilated buildings, *Energy and Buildings* 43 (1) (2011) 75–81. doi:10.1016/j.enbuild.2010.08.015.

751 [74] T. Chenvidyakarn, A. Woods, Multiple steady states in stack ventilation, *Building and Environment* 40 (3) (2005)  
752 399–410. doi:10.1016/j.buildenv.2004.06.020.

753 [75] J. Yuan, L. R. Glicksman, Multiple steady states in combined buoyancy and wind driven natural ventilation: The  
754 conditions for multiple solutions and the critical point for initial conditions, *Building and Environment* 43 (1)  
755 (2008) 62–69. doi:10.1016/j.buildenv.2006.11.035.

756 [76] N. B. Kaye, Y. Ji, M. J. Cook, Numerical simulation of transient flow development in a naturally ventilated room,  
757 *Building and Environment* 44 (5) (2009) 889–897. doi:10.1016/j.buildenv.2008.06.016.

758 [77] X. Faure, N. L. Roux, Time dependent flows in displacement ventilation considering the volume envelope heat  
759 transfers, *Building and Environment* 50 (2012) 221–230. doi:10.1016/j.buildenv.2011.11.007.

760 [78] D. Yang, Y. Guo, Fluctuation of natural ventilation induced by nonlinear coupling between buoy-  
761 ancy and thermal mass, *International Journal of Heat and Mass Transfer* 96 (2016) 218–230.  
762 doi:10.1016/j.ijheatmasstransfer.2016.01.017.

763 [79] D. Bastien, A. K. Athienitis, Passive thermal energy storage, part 1: Design concepts and metrics, *Renewable*  
764 *Energy* 115 (2018) 1319–1327. doi:10.1016/j.renene.2016.04.011.

765 [80] D. Bastien, A. K. Athienitis, Passive thermal energy storage, part 2: Design methodology for solaria and green-  
766 houses, *Renewable Energy* 103 (2017) 537–560. doi:10.1016/j.renene.2016.11.041.

767 [81] C. P. Underwood, An improved lumped parameter method for building thermal modelling, *Energy and Buildings*  
768 79 (2014) 191–201. doi:10.1016/j.enbuild.2014.05.001.

769 [82] R. Cheng, X. Wang, Y. Zhang, Analytical optimization of the transient thermal performance of building  
770 wall by using thermal impedance based on thermal-electric analogy, *Energy and Buildings* 80 (2014) 598–612.  
771 doi:10.1016/j.enbuild.2014.05.023.

772 [83] E. Mantesi, C. J. Hopfe, M. J. Cook, J. Glass, P. Strachan, The modelling gap: Quantifying the discrepancy  
773 in the representation of thermal mass in building simulation, *Building and Environment* 131 (2018) 74–98.  
774 doi:10.1016/j.buildenv.2017.12.017.

775 [84] W. H. Ko, S. Schiavon, G. Brager, B. Levitt, Ventilation, thermal and luminous autonomy metrics for an integrated

776 design process, *Building and Environment* 145 (2018) 153–165. doi:10.1016/j.buildenv.2018.08.038.

777 [85] A. Athienitis, W. O'Brien, *Modeling, Design, and Optimization of Net-Zero Energy Buildings*, John Wiley & Sons, 2015.

779 [86] J. Hillary, E. Walsh, A. Shah, R. Zhou, P. Walsh, Universal approach to modelling multi-layer structures in building  
780 energy simulations, *Energy and Buildings* 170 (2018) 122–133. doi:10.1016/j.enbuild.2018.04.009.

781 [87] L.-S. Wang, P. Ma, E. Hu, D. Giza-Sisson, G. Mueller, N. Guo, A study of building envelope and thermal  
782 mass requirements for achieving thermal autonomy in an office building, *Energy and Buildings* 78 (2014) 79–88.  
783 doi:10.1016/j.enbuild.2014.04.015.

784 [88] J. Hillary, E. Walsh, A. Shah, R. Zhou, P. Walsh, Guidelines for developing efficient thermal conduction and  
785 storage models within building energy simulations, *Energy* 125 (2017) 211–222. doi:10.1016/j.energy.2017.02.127.

786 [89] D. Alterman, T. Moffiet, S. Hands, A. Page, C. Luo, B. Moghtaderi, A concept for a potential met-  
787 ric to characterise the dynamic thermal performance of walls, *Energy and Buildings* 54 (2012) 52–60.  
788 doi:10.1016/j.enbuild.2012.08.006.

789 [90] B. M. Jones, M. J. Cook, S. D. Fitzgerald, C. R. Iddon, A review of ventilation opening area terminology, *Energy*  
790 and *Buildings* 118 (2016) 249–258. doi:10.1016/j.enbuild.2016.02.053.

791 [91] H. B. Awbi, A. Hatton, Mixed convection from heated room surfaces, *Energy and Buildings* 32 (2) (2000) 153–166.  
792 doi:10.1016/S0098-8472(99)00063-5.

793 [92] H. B. Awbi, Calculation of convective heat transfer coefficients of room surfaces for natural convection, *Energy*  
794 and *Buildings* 28 (2) (1998) 219–227. doi:10.1016/S0378-7788(98)00022-X.

795 [93] A. Novoselac, B. J. Burley, J. Srebric, New Convection Correlations for Cooled Ceiling Panels in Room with Mixed  
796 and Stratified Airflow, *HVAC&R Research* 12 (2) (2006) 279–294. doi:10.1080/10789669.2006.10391179.

797 [94] M. A. Menchaca-Brandan, F. A. D. Espinosa, L. R. Glicksman, The influence of radiation heat transfer on  
798 the prediction of air flows in rooms under natural ventilation, *Energy and Buildings* 138 (2017) 530–538.  
799 doi:10.1016/j.enbuild.2016.12.037.

800 [95] *Handbook of heat transfer*, McGraw-Hill, 1998.

801 [96] G. Nellis, S. A. Klein, *Heat transfer*, Cambridge University Press, Cambridge; New York, 2009.

802 [97] M. F. Ashby, *Materials and the environment : eco-informed material choice*, 2nd Edition, Elsevier/Butterworth-  
803 Heinemann, Amsterdam ; Boston, 2013.

804 [98] J. N. Hacker, T. P. D. Saulles, A. J. Minson, M. J. Holmes, Embodied and operational carbon dioxide emissions  
805 from housing: A case study on the effects of thermal mass and climate change, *Energy and Buildings* 40 (3) (2008)  
806 375–384. doi:10.1016/j.enbuild.2007.03.005.

807 [99] C. D. Perna, F. Stazi, A. U. Casalena, M. D'Orazio, Influence of the internal inertia of the building envelope  
808 on summertime comfort in buildings with high internal heat loads, *Energy and Buildings* 43 (1) (2011) 200–206.  
809 doi:10.1016/j.enbuild.2010.09.007.

810 [100] H. Wang, Q. Chen, A semi-empirical model for studying the impact of thermal mass and cost-  
811 return analysis on mixed-mode ventilation in office buildings, *Energy and Buildings* 67 (2013) 267–274.  
812 doi:10.1016/j.enbuild.2013.08.025.

813 [101] T. Wangler, N. Roussel, F. P. Bos, T. A. M. Salet, R. J. Flatt, *Digital Concrete: A Review*, *Cement and Concrete*

814 Research 123 (2019) 105780. doi:10.1016/j.cemconres.2019.105780.

815 [102] M. Popescu, L. Reiter, A. Liew, T. V. Mele, R. J. Flatt, P. Block, Building in Concrete with an Ultra-  
816 lightweight Knitted Stay-in-place Formwork: Prototype of a Concrete Shell Bridge, *Structures* 14 (2018) 322–332.  
817 doi:10.1016/j.istruc.2018.03.001.

818 [103] R. A. Buswell, W. R. L. de Silva, S. Z. Jones, J. Dirrenberger, 3D printing using concrete extrusion: A roadmap  
819 for research, *Cement and Concrete Research* 112 (2018) 37–49. doi:10.1016/j.cemconres.2018.05.006.

820 [104] S. J. Keating, J. C. Leland, L. Cai, N. Oxman, Toward site-specific and self-sufficient robotic fabrication on  
821 architectural scales, *Science Robotics* 2 (5) (2017) eaam8986. doi:10.1126/scirobotics.aam8986.

822 [105] M. West, *The Fabric Formwork Book: Methods for Building New Architectural and Structural Forms in Concrete*,  
823 Routledge, 2016.

824 [106] S. Adriaenssens, P. Block, D. Veenendaal, C. Williams, *Shell Structures for Architecture: Form Finding and  
825 Optimization*, Routledge, 2014.

826 [107] D. Veenendaal, M. West, P. Block, History and overview of fabric formwork: using fabrics for concrete casting,  
827 *Structural Concrete* 12 (3) (2011) 164–177. doi:10.1002/suco.201100014.

828 [108] J.-F. Bastin, Y. Finegold, C. Garcia, D. Mollicone, M. Rezende, D. Routh, C. M. Zohner, T. W. Crowther, The  
829 global tree restoration potential, *Science* 365 (6448) (2019) 76–79. doi:10.1126/science.aax0848.

830 [109] B. King, *The New Carbon Architecture: Building to Cool the Climate*, New Society Publishers, 2017.

831 [110] D. Wood, C. Vailati, A. Menges, M. Rüggeberg, Hygroscopically actuated wood elements for weather responsive  
832 and self-forming building parts – Facilitating upscaling and complex shape changes, *Construction and Building  
833 Materials* 165 (2018) 782–791. doi:10.1016/j.conbuildmat.2017.12.134.

834 [111] *Advancing Wood Architecture: A Computational Approach*, 1st Edition, Routledge, London ; New York, 2016.

835 [112] A. Laborel-Préneron, C. Magniont, J.-E. Aubert, Hygrothermal properties of unfired earth bricks: Effect  
836 of barley straw, hemp shiv and corn cob addition, *Energy and Buildings* 178 (2018) 265–278.  
837 doi:10.1016/j.enbuild.2018.08.021.

838 [113] D. U. Shah, M. C. D. Bock, H. Mulligan, M. H. Ramage, Thermal conductivity of engineered bamboo composites,  
839 *Journal of Materials Science* 51 (6) (2016) 2991–3002. doi:10.1007/s10853-015-9610-z.

840 [114] E. W. Weisstein, Legendre Polynomial.  
841 URL <http://mathworld.wolfram.com/LegendrePolynomial.html>

842 [115] E. W. Weisstein, Sierpiński Curve.  
843 URL <http://mathworld.wolfram.com/SierpinskiCurve.html>

844 [116] E. W. Weisstein, Cesàro Fractal.  
845 URL <http://mathworld.wolfram.com/CesaroFractal.html>

846 [117] E. W. Weisstein, Koch Snowflake.  
847 URL <http://mathworld.wolfram.com/KochSnowflake.html>